

Geochemistry, Geophysics, Geosystems

RESEARCH ARTICLE

10.1002/2015GC005754

Key Points:

- Pore water chemistry indicate AOM and organoclastic sulfate reduction
- AOM and organoclastic sulfate reduction influences delta $^{34}\text{S}_{\text{CRS}}$ values
- Deccan basalt and APGC contributed reactive iron in K-G basin

Correspondence to:

A. Mazumdar,
maninda@nio.org

Citation:

Peketi, A., A. Mazumdar, H. M. Joao, D. J. Patil, A. Usapkar, and P. Dewangan (2015), Coupled C-S-Fe geochemistry in a rapidly accumulating marine sedimentary system: Diagenetic and depositional implications, *Geochem. Geophys. Geosyst.*, 16, 2865–2883, doi:10.1002/2015GC005754.

Received 27 JAN 2015

Accepted 4 AUG 2015

Accepted article online 7 AUG 2015

Published online 5 SEP 2015

Coupled C-S-Fe geochemistry in a rapidly accumulating marine sedimentary system: Diagenetic and depositional implications

A. Peketi¹, A. Mazumdar¹, H. M. Joao¹, D. J. Patil², A. Usapkar¹, and P. Dewangan¹

¹Geological Oceanography, CSIR-National Institute of Oceanography, Dona Paula, Goa, India, ²CSIR-National Geophysical Research Institute, Hyderabad, India

Abstract In the present study, we have investigated the C-S-Fe systematics in a sediment core (MD161-13) from the Krishna-Godavari (K-G) basin, Bay of Bengal. The core covers the late Holocene period with high overall sedimentation rate of $\sim 573 \text{ cm kyr}^{-1}$. Pore fluid chemical analyses indicate that the depth of the present sulfate methane transition zone (SMTZ) is at $\sim 6 \text{ mbsf}$. The $(\Delta\text{TA} + \Delta\text{Ca} + \Delta\text{Mg})/\Delta\text{SO}_4^{2-}$ ratios suggest that both organoclastic degradation and anaerobic oxidation of methane (AOM) drive sulfate reduction at the study site. The positive correlation between total organic carbon content (TOC) and chromium reducible sulfur (CRS) content indicates marked influence of organoclastic sulfate reduction on sulfidization. Coupled occurrence of ^{34}S -enriched iron sulfide (pyrite) with ^{12}C -enriched authigenic carbonate zones is the possible records of paleo-sulfate methane transition zones where AOM-driven-focused sulfate reduction was likely fueled by sustained high methane flux from underlying gas-rich zone. Aluminum normalized poorly reactive iron ($\text{Fe}_{\text{PR}}/\text{Al}$) and La/Yb ratios suggest increasing contribution from Deccan basalts relative to that of Archean-Proterozoic granitic complex in sediment flux of Krishna-Godavari basin during the last 4 kyr.

1. Introduction

Dissimilatory sulfate reduction [Madigan *et al.*, 2000; Canfield, 2001; Goldhaber, 2003; Megonigal *et al.*, 2003; Shen and Buick, 2004; Canfield *et al.*, 2005, 2006; Bradley *et al.*, 2011; Eckert *et al.*, 2011; Acosta *et al.*, 2014; Bowles *et al.*, 2014; Treude *et al.*, 2014] is a bacterially mediated metabolic process where dissolved sulfate is utilized as an electron acceptor during organic matter remineralization, and in this process sulfate is reduced to hydrogen sulfide. Sulfate reduction involves change of the valence state of sulfur from +6 to -2, i.e., a net transfer of eight electrons via enzymatic pathways [Canfield, 2001]. Several sulfur compounds of intermediate valence states like sulfite (SO_3^{2-}), tetrathionate ($\text{S}_4\text{O}_6^{2-}$), thiosulfate ($\text{S}_2\text{O}_3^{2-}$), and elemental sulfur (S^0) [Zopfi *et al.*, 2004] are known to exist in the sediment pore waters. During bacterial sulfate reduction, sulfate reducing bacteria preferentially breaks down the $^{32}\text{S}-^{16}\text{O}$ bond than $^{34}\text{S}-^{18}\text{O}$ as the energy required to break $^{32}\text{S}-^{16}\text{O}$ bond is lower than that for $^{34}\text{S}-^{18}\text{O}$ [Harrison and Thode, 1958; Lloyd, 1968]. This preferential consumption of lighter isotopes during sulfate reduction results in the enrichment of residual sulfate in ^{34}S relative to ^{32}S . Sulfate reducing bacteria (SRBs) are strict anaerobes and proliferate only in complete absence of oxygen. SRB are most active close to the sediment surface owing to high organic load and sulfate flux [Kasten and Jørgensen, 2000; Megonigal *et al.*, 2003; Jørgensen and Kasten, 2006; Jørgensen and Parkes, 2010; Meister *et al.*, 2013]. Preservation of labile organic matter and its availability to the sulfate reducers depend on oxygen penetration depth, which in turn is controlled by sedimentation rate oxygen availability and bioturbation [Hedges and Keil, 1995; Hartnett *et al.*, 1998; Kristensen, 2000; Gélinas *et al.*, 2001]. The free energy yield (ΔG) during sulfate reduction depends on the nature of electron donors (substrate). Fermentation products such as acetate, lactate, formate, and hydrogen are the common substrates in organic rich sediments for which Brüchert [2004] compiled a range of ΔG values (-45 to -340 kJ mol^{-1} SO_4^{2-}). However, recently Treude *et al.* [2014] observed that the “the classical redox cascade of electron acceptor utilization based on Gibbs energy yields does not always hold in diffusion-dominated systems, and instead biotic processes may be more strongly coupled to mineralogy.”

The rate of sulfate reduction depends on the availability of labile organic compounds (substrate for sulfate reducing bacteria), temperature, sedimentation rate, and sulfate concentrations [Goldhaber and Kaplan, 1975;

Berner, 1978; Westrich and Berner, 1988; Canfield, 1989a; Madigan *et al.*, 2000; Canfield, 2001; Detmers *et al.*, 2001; Claypool, 2004; Canfield *et al.*, 2005, 2006; Acosta *et al.*, 2014]. Dissimilatory sulfate reduction plays an extremely important role in marine sediment diagenesis and accounts for half or more of the total organic carbon mineralization within sediments [JØrgensen, 1982; Canfield, 1989a; Kristensen, 2000; Bowles *et al.*, 2014]. Advective/diffusive methane flux also plays a profound role in sulfate reduction in the sediments via anaerobic oxidation of methane (AOM) [Niewöhner *et al.*, 1998; Borowski *et al.*, 1996, 1999; Hoehler *et al.*, 2000]. AOM takes place within the sulfate methane transition zone (SMTZ) where both sulfate and methane concentration profiles intersect each other. AOM is performed by a syntrophic consortium of methane oxidizing archaea (ANME) and sulfate reducing bacteria [Boetius *et al.*, 2000; Orphan *et al.*, 2001; Reeburgh, 2007; Knittel and Boetius, 2009; Milucka *et al.*, 2012; Yoshinaga *et al.*, 2014]. Recently, Treude *et al.* [2014] proposed possible involvement of unknown phylotypes in AOM processes.

H_2S produced during sulfate reduction is trapped in the sediment as iron monosulfide (FeS), pyrite (FeS_2), elemental sulfur (S^0), and organic bound sulfur (OBS) out of which pyrite and OBS are quantitatively the most significant sinks of reduced sulfur in the marine environment [Kump and Garrels, 1986; Werne *et al.*, 2003; Holmkvist *et al.*, 2014]. A fraction of H_2S may diffuse out of the sediment and gets oxidized to sulfate or trapped in the bacterial mats as S^0 [Hansen *et al.*, 1978; Chanton *et al.*, 1987]. Sulfidization of sedimentary reactive iron has been studied in a wide variety of depositional environments [Skyring, 1987; Roychoudhury *et al.*, 2003; Mazumdar *et al.*, 2012b] across the geological time scale [Strauss, 1997].

In the present study, an attempt has been made to decipher the role of AOM and organoclastic sulfate reduction on sulfur isotope ratios of sulfides precipitated in the rapidly deposited marine sediments of the Krishna-Godavari (K-G) basin, Bay of Bengal. We have also tried to understand the reactive iron source variations using iron speciation studies.

2. Geology

The Krishna-Godavari basin is a pericratonic rift basin located in the eastern continental margin of India (ECMI), covering an area of 28,000 km² onshore and 145,000 km² offshore [Rao, 2001; Bastia, 2007]. Geographically, it lies between Kakinada in the northeast and Ongole in the southwest of Andhra Pradesh. The ECMI represents a passive continental margin and evolved through the breakup of the eastern Gondwana landmass 130 Ma ago when India separated from East Antarctica [Ramana *et al.*, 2001]. The initial rifting and drifting phase during the Cretaceous resulted in extensive deposition of fluvio-lacustrine sediments throughout the basin. A south-easterly tilt in late Cretaceous resulted in an extensive marine transgression which led to the deposition of the Ragavapuram formation [Sastri *et al.*, 1981; Rao and Mani, 1993]. The Ragavapuram formation (shale) is overlain successively by Razole Formation, Palakollu Shale, Vadaparru shale, Narsapur Claystone, Ravva Formation, and Godavari clay. The Godavari clay ranges in age from mid-Pliocene to Holocene. The basin extends southeast into the deep waters of the Bay of Bengal. The basin is characterized by enechelon type horst and graben-like structures [Rao and Mani, 1993; Rao, 2001; Gupta, 2006]. A sediment thickness of 3–5 km in the onshore region and around 8 km in the offshore region has been reported by Bastia [2007] and Prabhakar and Zutshi [1993]. The mean annual sediment transportation of the Krishna and Godavari rivers are estimated to be 67.7 and 170×10^6 metric ton respectively [Biksham and Subramanian, 1988; Ramesh and Subramanian, 1988]. Tropical semiarid climatic conditions prevail in most parts of the catchment area. The catchment area is occupied by Archaean-Proterozoic granitic complex, Tertiary Deccan traps (basaltic) and recent sediments [Ramesh and Subramanian, 1988; Biksham and Subramanian, 1988; Mazumdar *et al.*, 2014a].

The high-resolution sparker (HRS) data [Mazumdar *et al.*, 2012a] in the vicinity of MD161-13 (Figure 1) show distinct surface echo with several parallel, continuous subbottom reflections that are conformable to sea-floor topography. Regional and counter growth faults are also common in this region which may be attributed to shale tectonics [Dewangan *et al.*, 2010]. The acoustic signature of gas movement, such as acoustic voids is also observed within the layered structures of MD161-13 [Mazumdar *et al.*, 2012a]. The hydrate stability zone calculation and the absence of a bottom simulating reflector suggest that the study area is located outside the gas hydrate stability zone in the K-G basin (NIO, Geoscientific investigations of shallow sediments in Krishna Godavari, East Coast, unpublished NIO Tech. Rep. 12–2003, p. 84, Natl. Gas Hydrate Res. Program, 2005, Goa, India).

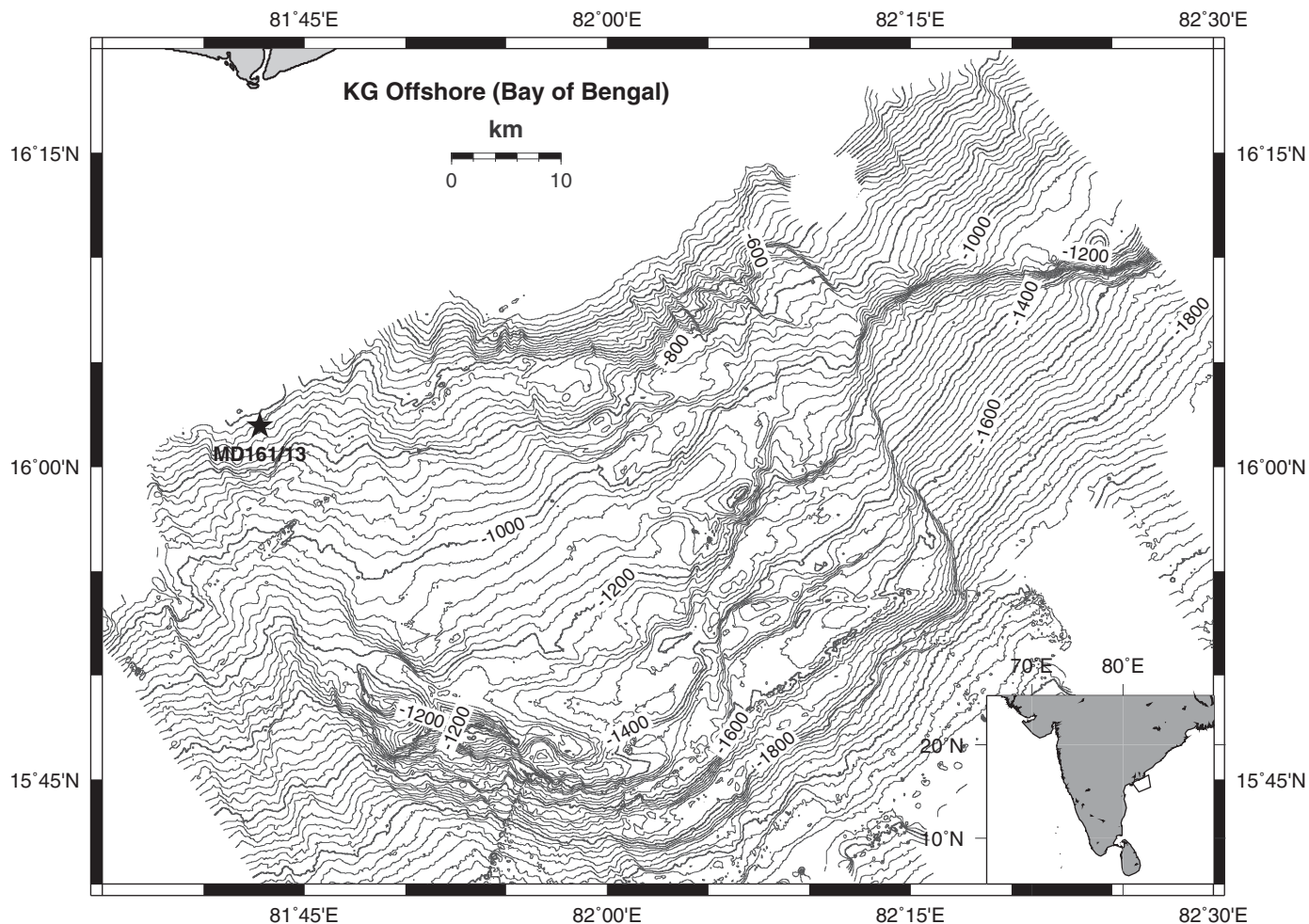


Figure 1. Bathymetry map displaying location of core MD161-13 (star). The inset shows partial map of India along with the study area in the Krishna-Godavari basin.

3. Methodology

3.1. Geochemical Measurements

A 28.65 m long sediment core MD161-13 (Figure 1) was collected on board *Marion Dufresne* (May 2007) at a water depth of 647 m (Lat.: 16°01.9684 N, Long.: 81°42.7909 E) using a giant Calypso piston corer. PVC liners of 10 cm inner diameter were used for core collection. Subsampling for pore water extraction was carried out by cutting out 10 cm thick sediment slabs at 1.5 m interval within 1.5 h after core retrieval. Subsampling for gas was carried out using a 10 mL cut-syringe from the core of the sediment slabs to minimize atmospheric contamination. The aliquot was stored in 28 mL glass vials with 5 mL of 0.5 M sodium azide (bactericides) and crimped immediately following nitrogen flushing. Sediment was homogenized using a vortex shaker and stored at 2°C till concentrations of hydrocarbon (CH_4 , C_2H_6 , and C_3H_8) gases in the head space were measured using a Varian Gas chromatograph (CP 3380). Stable carbon isotope ratios of head space methane and carbon dioxide were measured with a Finnigan-Delta Plus Isotope Ratio Mass Spectrometer in continuous flow mode interfaced to a gas chromatograph.

After subsampling for gas concentration measurements, sediment slabs were immediately transferred into thick plastic bags, filled with high-purity nitrogen and heat sealed to avoid atmospheric oxygen contamination which can oxidize hydrogen sulfide/iron monosulfide and stored at 4°C. Pore water was extracted from the sediment using a Manheim-type hydraulic press following standard ODP protocol [Sayles et al., 1973]. Pore waters were collected in 20 mL plastic syringes with Luer locks, filtered through a 0.2 μm Whatman syringe filter and stored in crimp vials under nitrogen head and preserved at 2°C. Total alkalinity was

measured on board following the Gran titration method using a Metrohm Autotitrator (Titrino 799 GPT). Sulfate concentrations were measured using a Dionex-600 ion chromatograph [Gieskes *et al.*, 1991]. Prior to sample injection, 1 mL of pore water sample was diluted to 50 or 100 mL and passed through a silver cartridge to remove chloride ions. An IonPac AS9-HC column was used for ion separation and ASRS Ultra-II (2 mm) was used as anion self-regenerating suppressor. Calibration curve was prepared using a standard IC sulfate solution from Dionex. The calibration line was cross checked with Dionex anion mixed standard. A precision of 0.5–1% is reported here. BaCl₂ solution was added to the filtered acidified pore water to precipitate the dissolved sulfate as BaSO₄. BaSO₄ was recovered by filtration and dried for sulfur isotope ratio measurement. Calcium and magnesium concentrations in the pore waters were measured using an ICP-AES (Model: Thermo Electron IRIS INTREPID II XSP DUO). The precision of 1% is reported for calcium and magnesium concentration measurements.

For the solid-phase analyses, the core was subsampled at 20–50 cm interval. S⁰ was extracted from an aliquot of homogenized wet sample by shaking it with dichloromethane on a vortex shaker [Brüchert and Pratt, 1996; Brüchert, 1998] and dichloromethane was removed by centrifugation. Sediment water content was determined by weight loss upon drying overnight at 65°C for correction of the data to dry weight basis [Cornwell and Morse, 1987]. Acid volatile sulfur (AVS) and chromium reducible sulfur (CRS) were extracted from the S⁰-free sediment following a two-step extraction using 6 N HCl and 1 M CrCl₂ sequentially in an oxygen-free chamber with continuous nitrogen flow. CRS contents in this work represent the pyrite-bound sulfur content in the sediment samples. H₂S produced by reduction of sulfides was trapped as ZnS in zinc acetate solution (pH > 11) and subsequently reprecipitated as Ag₂S by addition of AgNO₃ [Canfield *et al.*, 1986; Strauss *et al.*, 2012]. δ³⁴S, δ¹⁸O of BaSO₄, and δ³⁴S of Ag₂S were measured with a Thermo Delta-V-plus isotope ratio mass spectrometer in continuous flow mode coupled with an elemental analyzer (Thermo EA-1112). BaSO₄ and Ag₂S precipitates were mixed with V₂O₅ and combusted at 1150°C to produce SO₂. Whereas, oxygen isotope ratio measurements of BaSO₄ were carried out following pyrolysis of BaSO₄ to CO. Pyrolysis was carried out in glassy carbon reactor at 1450°C. All results are reported in the standard delta notation as permil deviations from the VCDT (Vienna Canyon Diablo Troilite) and VSMOW (Vienna Standard Mean Ocean Water) with reproducibility better than ±0.3‰ for S and O isotope ratios. IAEA standards SO-5 (BaSO₄, δ³⁴S: +0.5‰ VCDT and δ¹⁸O: +12‰ VSMOW), SO-6 (BaSO₄, δ³⁴S: -34.1‰ VCDT and δ¹⁸O: -11‰ VSMOW), NBS127 (BaSO₄, δ³⁴S: +22.3‰ VCDT and δ¹⁸O: +9.3‰ VSMOW), S-1 (Ag₂S, δ³⁴S: -0.3‰ VCDT), and S-2 (Ag₂S, δ³⁴S: +22.7‰ VCDT) were used for the preparation of calibration curves.

The dithionite leachable iron (Fe_D) in the sediment including ferrihydrite (FeOOH·0.4H₂O), lepidocrocite (γ-FeOOH), goethite (FeOOH), and hematite (Fe₂O₃) was extracted with buffered sodium dithionite solution following Mehra and Jackson [1960] and Canfield [1989b]. Iron concentrations (Fe³⁺ + Fe²⁺) were measured by ferrozine complexometry following reduction of Fe³⁺ to Fe²⁺ by addition of hydroxylamine hydrochloride in the leachate. A Chemito spectrophotometer (Spectroscan UV 2700) was used to measure absorbance at 515 nm. Another aliquot of sediment was subjected to dithionite leaching and the Fe_D-free residual sediment was leached for 6 h with 0.2 M ammonium oxalate solution at 3.2 pH to extract the magnetite bound iron (Fe_{Ox}) [McKeague and Day, 1966; Poulton and Canfield, 2005; Chen *et al.*, 2013]. Iron concentrations in the leachate were measured with an Atomic Absorption Spectrophotometry (Varian: Varian AA240FS). Standard reproducibility for Fe is 0.3%. Calibration line was prepared with Merck iron standard. The highly reactive iron (Fe_{HR}) is the sum of Fe_{Ox}, Fe_D, and pyrite-bound iron (Fe_{CRS}). Total iron and aluminum contents in freeze-dried bulk sediment samples (desalinated) were determined by X-ray Fluorescence (PAN analytical Axios) technique using fused pellets. A standard reproducibility of ±3% is reported in this work.

Total inorganic carbon (TIC) contents were determined by a carbon coulometer (UIC-CM5130). Total carbon (TC) content was measured by elemental analyzer (Thermo EA1112). Total organic carbon (TOC) was calculated by subtracting TIC from TC. Ultrapure CaCO₃ (Sigma-Aldrich) was used as standard for TIC measurement. Precision for TC and TIC measurements are 1 and 1.4%, respectively. Stable carbon and oxygen isotope ratios of carbonate in bulk sediments were determined with a Thermo Delta V continuous flow isotope ratio mass spectrometer coupled to a GASBENCH-II and PAL auto sampler at the National Geophysical Research Institute (Hyderabad, India). The isotope ratios are reported in standard delta notation as permil deviations from VPDB standard. A sample reproducibility of 0.1‰ for both carbon is reported here.

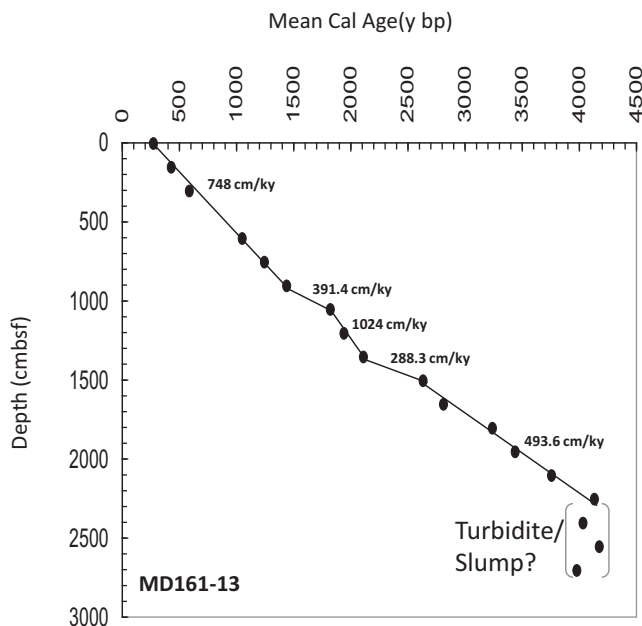


Figure 2. Age model for MD161-13.

Rare earth element concentrations were measured following Li-metaborate/tetraborate fusion method at Actlabs, Canada. Fused samples were dissolved in nitric acid and concentrations were measured using an ICP-MS. The accuracy of the data was better than $\pm 6\%$.

AMS ^{14}C dates were generated at the National Ocean Sciences AMS (NOSAMS) facility, Woods Hole Oceanographic Institution, USA. Dates were determined on planktonic foraminifera of the species *Globigerinoides ruber* and *Globigerinoides sacculifer*. Carbon dioxide generated from these foraminifera shells was reacted with catalyst to form graphite which was pressed into targets and analyzed on the accelerator along with standards and process blanks. Two primary standards used during ^{14}C measurements are NBS Oxalic Acid I (NIST-SRM-4990) and Oxalic Acid II (NIST-SRM-4990C).

3.2. Flux Calculation

The diffusive sulfate flux (J_{SO_4}) is calculated from concentration profiles using Fick's first law (equation (1)) assuming steady state conditions [Berner, 1980; Canfield, 1989a, 1991]

$$J_{\text{SO}_4} = \varphi D_s (dC/dX) \quad (1)$$

where J_{SO_4} , C , and φ represent the depth-integrated sulfate reduction rate ($\text{mmol m}^{-2} \text{yr}^{-1}$), sulfate concentration (mM) in the pore water, and average sediment porosity, respectively. dC/dX is the sulfate concentration gradient and D_s ($\text{cm}^2 \text{s}^{-1}$) is the molecular diffusivity corrected for tortuosity. D_s is calculated by the formula:

$$D_s = D_o / [1 + n(1 - \varphi)] \quad (2)$$

where $n = 3$ for clays and silt [Iversen and JØrgensen, 1993]. D_o = sulfate diffusivity in the absence of particles. Since D_o varies with temperature (water depth), we have calculated D_o at different temperatures using an empirical relation based on data set from Li and Gregory [1974].

3.3. Magnetic Measurement

Magnetic susceptibility measurement was performed using a Bartington MS2B dual frequency susceptibility meter. Susceptibility measurements (χ_{LF}) were done at a frequency of 0.47 kHz.

4. Results

4.1. Age Model

The age-depth relationship of the core MD161-13 is given in Figure 2. Radiocarbon ages are converted to mean calendar ages using a radio carbon calibration program [Fairbanks et al., 2005]. The sedimentation rates range from 288 to 1024 cm kyr^{-1} . The overall sedimentation rate based on the slope of the regression line passing through all the data points is 573 cm kyr^{-1} . Below 23.0 mbsf, the age reversals indicate possible turbidite layers or slumping. Results of solid-phase analysis are thus restricted to 22.65 mbsf only.

4.2. Pore Fluid Concentrations and Isotope Ratio Profiles

The composition and isotope ratios of head space gases and sediment pore waters of the core MD161-13 are presented in Table 1. The concentration profiles of sulfate-methane-alkalinity are plotted in Figure 3a.

Table 1. Concentrations and Isotope Ratios of Various Dissolved Components in the Pore Waters and Head Space Gases^a

Depth (mbsf)	SO ₄ (mM)	TA (mM)	CH ₄ (μM)	C1/(C2 + C3)	δ ¹³ C CH ₄ (‰ VPDB)	δ ¹³ C CO ₂ (‰ VPDB)	Ca (mM)	Mg (mM)	δ ³⁴ S _{SO4} Pw (‰ VCDT)	δ ¹⁸ O _{SO4} Pw (‰ VSMOW)
0.05	26.5	7.4	4.3	10.8	-37.3	-17.7	10.5	55.0	27.7	12.9
1.55	16.1	18.6	3.6	40.9	-40.4	-19.8	8.9	53.5	53.8	24.3
3.055	10.7	21.8		14.1			7.5	51.6	71.4	
4.55	6.9	25.2	1.8	16.4	-27.3	-18.9	7.6	49.6	92.4	25.2
6.055	0.2	25.8					7.1	51.6		
7.55	nd	22.0	6.0	43.0	-65.8	-13.7				
9.055	nd	10.3	44.8	328.6	-90.9	-17.1	5.3	46.6		
10.55	nd	7.4	90.1	313.3			5.7	48.3		
12.055	nd	6.6					5.3	46.2		
13.55	nd	8.0	283.2	608.6	-98.2	-17.7	6.1	48.4		
15.055	nd	8.6					5.2	49.2		
16.55	nd	10.5	839.5	775.3			6.2	51.1		
18.055	nd	7.8								
19.55	nd	7.3	1930.0	1666.8	-95.2	-15.2	5.4	48.1		
21.055	nd	6.9					5.1	48.4		
22.55	nd	5.9	2440.7	1527.9	-92.9	-15.4				
24.055	nd	6.2					4.8	46.2		
25.55	nd	5.8	4941.0	2910.8	-92.5	-15.9	4.5	44.7		
27.055	nd	6.4					4.9	47.1		
28.55	nd	5.4					5.0	46.3		

^and = not detected.

The sulfate concentration profile is quasi-linear, whereas the methane concentration profile is concave-up in nature. Total alkalinity (TA) profile shows an approximate parabolic shape that is symmetrical across the SMTZ. TA reaches a maximum of 25.8 mM at the SMTZ. The sulfate concentration gradient is 0.041 mM/cm and J_{SO_4} is 28.6 mmol m⁻² yr⁻¹. The depth of the SMTZ is ~6 mbsf. The methane concentrations increase sharply below the SMTZ. Head space methane concentration (Figure 3a; Table 1) is close to the detection limit (4–6 μM) within top 7.55 mbsf and increases steadily to 4941 μM below the SMTZ. Below the SMTZ, C₁/(C₂ + C₃) ratio increases to the maximum of 2910. C₁, C₂, and C₃ represent methane, ethane, and propane concentrations, respectively. δ¹³C_{CH4} varies from -98.2 to -65.8‰ VPDB below the SMTZ (Figure 3b). Whereas, above SMTZ, δ¹³C_{CH4} fluctuates between -40.4 and -27.3‰, δ¹³C_{CO2} ranges from -19.8 to -13.7‰. δ³⁴S_{SO4} increases systematically down core (0.05–4.55 mbsf) from +27.7 to +92.4‰ and the corresponding δ¹⁸O_{SO4} values increases from +12.9 to +25.2‰ (Figure 3c). The Ca concentration decreases steadily with depth from 10.5 mM at the core top to 5.3 mM at a depth of 9.05 mbsf. Below 9.05 mbsf, the Ca concentration fluctuates between 4.5 and 6.2 mM (Table 1). The Mg concentration drops from 55 mM at the core top to 46 mM at 9.05 mbsf. Below 9.05 mbsf, Mg concentration fluctuates between 44.7 and 49.2 mM. The (ΔTA + ΔCa + ΔMg)/ΔSO₄²⁻ ratio drops with depth from 2.5 to 1 from core top to the SMTZ, respectively (Figure 4).

4.3. Solid-Phase S-C-Fe Concentrations and Isotope Ratios

CRS contents in core MD161-13 vary between 0.005 to 0.26 wt % (Table 2) and increase with depth below the sediment surface (Figure 5a). The CRS and the TOC profiles show marked coherence (Figure 5a). The TOC contents range from 0.7 to 2.4 wt % and show a positive correlation ($r^2 = 0.7$) with CRS contents (Figure 5b). S⁰ and AVS contents in all the samples are below detection limit. δ³⁴S_{CRS} values show wide variation ranging from -28.7 to +33.1‰ VCDT. The lowest δ³⁴S_{CRS} is recorded at a depth of 0.85 mbsf, whereas the highest δ³⁴S_{CRS} is observed at the depth of 9.15 mbsf. Within the top 9.15 mbsf, δ³⁴S_{CRS} gradually increases down core with large positive shifts to +3‰ at a depth of 8.7 mbsf which is followed by a zone (9.15–10.15 mbsf) of ³⁴S-enriched (+26.6 to 33.1‰) values. This zone is followed by a downward decrease in δ³⁴S_{CRS} in the 10–16 m depth interval (Figure 6a). Below 16 m, δ³⁴S_{CRS} again increases down core with a sharp positive δ³⁴S peak at 18.15 mbsf.

The δ¹³C_{TIC} values vary from -7.6 to -3.3‰ VPDB. The δ¹³C_{TIC} profile shows two broad zones of depletions (Figure 6b) and an overall inverse relationship with δ³⁴S_{CRS}.

Dithionite extractable (Fe_D) and oxalate extractable iron (Fe_{Ox}) range from 0.73 to 1.31 and 0.36 to 0.64 wt %, respectively. Whereas, Fe_{CRS} content varies from 0.005 to 0.233 wt %. Highly reactive iron contents

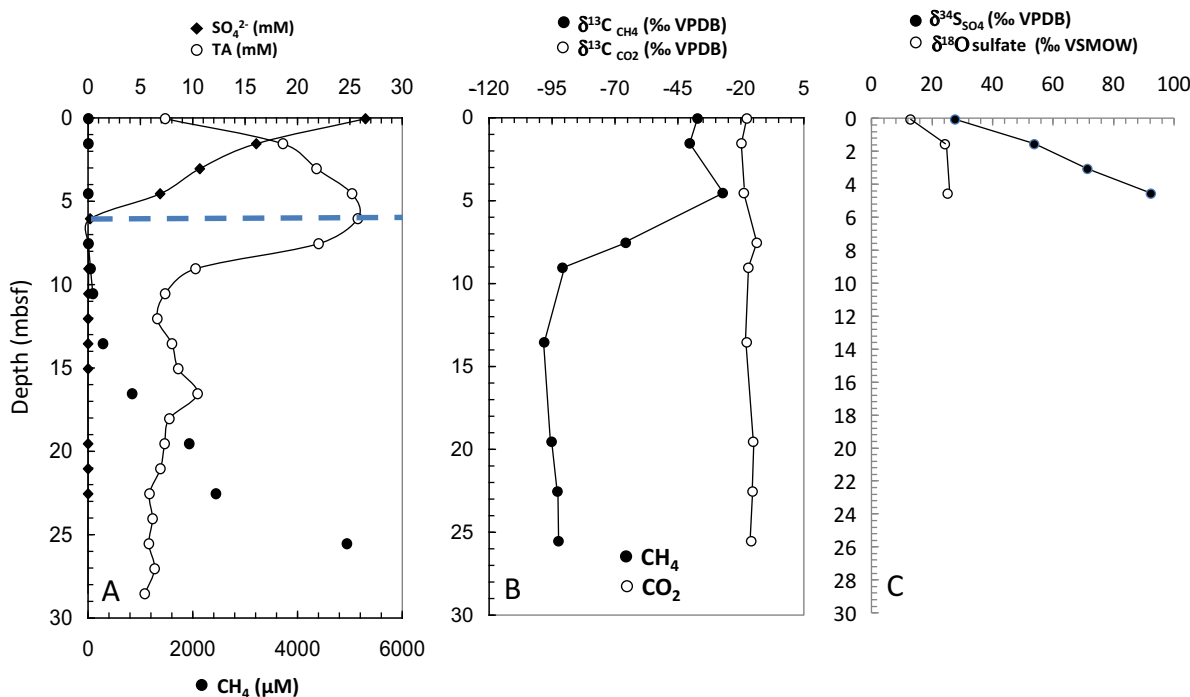


Figure 3. (a) Sulfate, total alkalinity (TA), and methane concentration profiles. (b) Carbon isotope ratios of headspace CO_2 and CH_4 gases. (c) Sulfur and oxygen isotope ratios of pore water sulfate.

vary from 1.33 to 1.85 wt % (Table 2). The Fe_{HR} is defined here as the fraction of sediment iron which has relatively low sulfidation half-lives compared to the silicate bound iron [Canfield *et al.*, 1992; Raiswell, 1997; Poulton *et al.*, 2004]. Dithionite extractable iron (Fe_{D}) is the major component of Fe_{HR} . The degree of pyritization ($\text{Fe}_{\text{CRS}}/\text{Fe}_{\text{HR}}$ %) ranges from 1.33 to 17.55% and increases with depth (Figure 7a and Table 2). Total iron content (Fe_{T}) varies from 6.5 to 8.1 wt % with an average of 7.5 ± 0.4 wt % (Table 2).

Fe_{HR} shows an overall positive relationship with the Fe_{T} content (Figure 8). The $\text{Fe}_{\text{HR}}/\text{Fe}_{\text{T}}$ ratio varies from 0.184 to 0.244 (Avg. 0.22 ± 0.01). The poorly reactive iron content ($\text{Fe}_{\text{PR}} = \text{Fe}_{\text{T}} - \text{Fe}_{\text{HR}}$) ranges from 5.12 to 6.52 wt %. The poorly reactive iron include the sheet silicates and unreactive Fe bearing phases like illmenite, garnet, augite, and amphiboles [Canfield *et al.*, 1992; Poulton and Raiswell, 2002]. The aluminum content ranges from 7.2 to 8.9 wt %. The $\text{Fe}_{\text{PR}}/\text{Al}$ ratio varies from 0.61 to 0.83 (Avg. 0.73 ± 0.05).

The magnetic susceptibility ranges from 0.6 to $1.4 \times 10^{-6} \text{ m}^3 \text{ kg}^{-1}$. The magnetic susceptibility decreases down core except a broad zone of enhancement within 15.32–18.65 mbsf highlighted in Figure 7b.

Lanthanum (La) and Yb concentrations range from 23.3 to 37.3 and 2.1 to 2.6 ppm, respectively. The La/Yb ratio ranges from 10.6 to 16 (Figure 9 and Table 3).

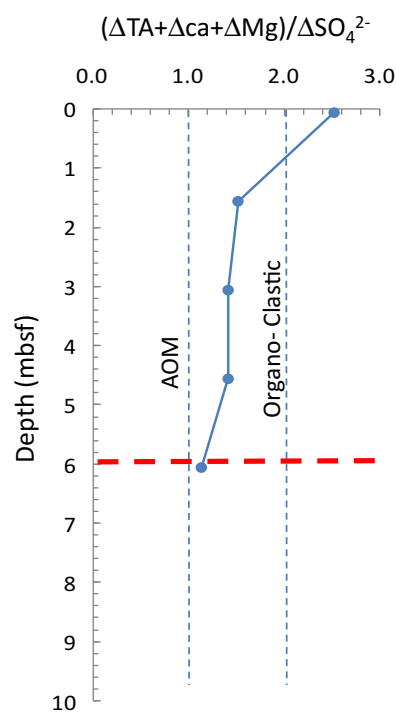


Figure 4. Vertical profile of pore water $(\Delta\text{TA} + \Delta\text{Ca} + \Delta\text{Mg})/\Delta\text{SO}_4^{2-}$ ratios.

5. Discussion

5.1. Methanogenesis

Highly depleted carbon isotopic compositions (Figure 3b; Table 1) of methane (−98.2 to −65.8 ‰) and high $\text{C}_1/(\text{C}_2 + \text{C}_3)$ ratios (2910) below the SMTZ indicate a microbial origin of methane at

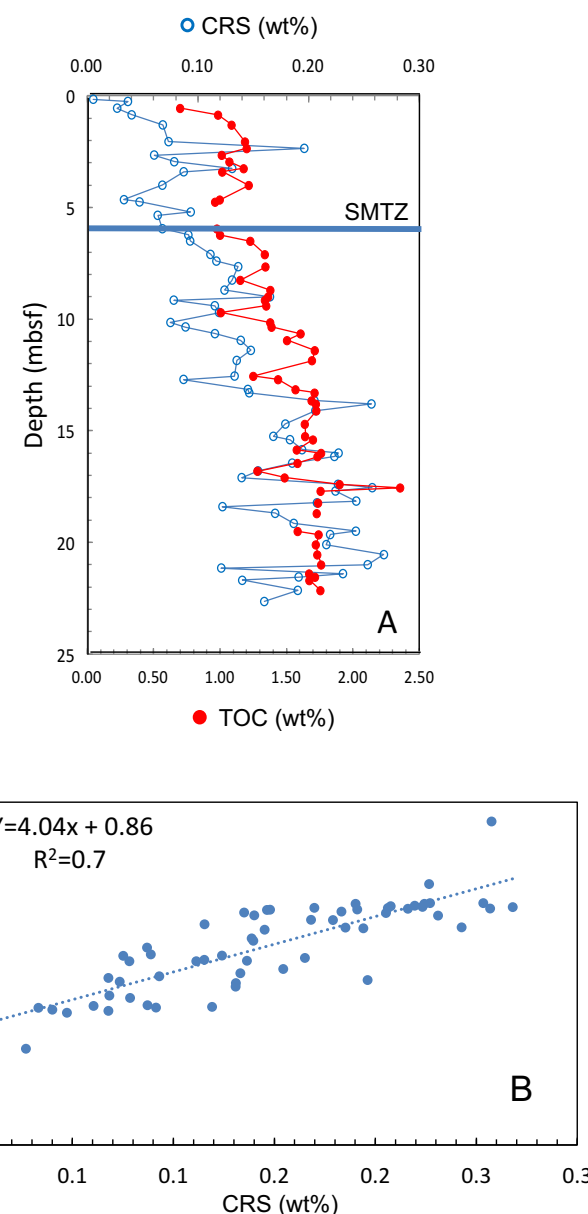
Table 2. Concentrations and Isotope Ratios of Various Components in the Bulk Sediment

Age (kyr BP)	Depth (mbsf)	CRS (wt %)	$\delta^{34}\text{S}_{\text{CRS}}$ (‰ VCDT)	Fe_{CRS} (wt%)	Fe_{D} (wt %)	Fe_{Ox} (wt %)	Fe_{HR}	Fe_{T} (wt %)	$\text{Fe}_{\text{HR}}/\text{Fe}_{\text{T}}$	DOP (%)	Fe_{PR} (wt %)	AI (wt %)	$^{13}\text{C}_{\text{TIC}}$ (‰ VPDB)	TOC (wt %)	$\text{Fe}_{\text{PR}}/\text{AI}$
0.25	0.15	0.0054	-27.6	0.005											
0.26	0.25	0.0367	-24.7	0.032	1.30	0.40	1.74	7.8	0.22	1.84	6.05	8.09	-3.4	0.748	
0.30	0.55	0.0270	-14.3	0.024	1.31	0.43	1.76	7.7	0.23	1.33	5.90	7.29	-5.1	0.70	
0.34	0.85	0.0401	-28.7	0.035	1.23	0.43	1.70	8.0	0.21	2.06	6.27	8.42	-3.6	0.99	
0.40	1.3	0.0682	-27.8	0.059	1.29	0.38	1.73	7.9	0.22	3.44	6.13	7.58	-3.3	1.09	
0.50	2.05	0.0734	-23.2	0.064	1.16	0.39	1.61	7.7	0.21	3.97	6.10	8.08	-4.3	1.19	
0.54	2.35	0.1961	-25.6	0.171	1.26	0.40	1.83	7.9	0.23	9.33	6.10	7.84	-3.7	1.20	
0.58	2.65	0.0604	-22.4	0.053	1.16	0.46	1.67	7.7	0.22	3.15	6.02	8.17	-3.8	1.01	
0.62	2.95	0.0786	-18.5	0.068	1.07	0.41	1.56	7.7	0.20	4.40	6.17	7.68	-4.3	1.07	
0.66	3.25	0.1309	-23.2	0.114	1.14	0.37	1.63	7.9	0.21	7.00	6.25	7.79	-3.9	1.18	
0.68	3.4	0.0871	-20.0	0.076		0.40		7.8					-4.0	1.02	
0.77	4	0.0679	-22.8	0.059	1.18	0.48	1.72	7.9	0.22	3.44	6.18	8.13	-4.0	1.22	
0.85	4.65	0.0332	-15.4	0.029									1.00		
0.87	4.75	0.0472	-22.6	0.041	1.18	0.39	1.61	7.8	0.21	2.56	6.19	8.51	-4.1	0.96	
0.93	5.2	0.0935	-16.7	0.081	1.16	0.57	1.80	7.8	0.23	4.51	5.99	7.83	-4.0	0.764	
0.95	5.35	0.0636	-8.6	0.055	1.10	0.46	1.61	7.7	0.21	3.45	6.06	7.24	-4.3	0.837	
1.03	5.95	0.0679	-3.0	0.059	1.10	0.55	1.71	7.7	0.22	3.46	5.98	8.09	-4.0	0.98	
1.06	6.23	0.0913	-11.2	0.080	1.15	0.39	1.61	7.7	0.21	4.93	6.10	8.06	-4.1	1.00	
1.10	6.5	0.0930	-6.7	0.081	1.13	0.45	1.66	7.9	0.21	4.89	6.22	8.06	-3.9	1.23	
1.18	7.1	0.1113	-6.3	0.097	1.06	0.49	1.65	7.8	0.21	5.86	6.14	8.11	-4.1	1.34	
1.22	7.4	0.1167	2.8	0.102	1.04	0.64	1.78	7.9	0.22	5.71	6.14	8.11	-4.3	0.757	
1.25	7.65	0.1364	1.6	0.119	1.11	0.49	1.72	7.8	0.22	6.91	6.09	8.36	-4.1	1.34	
1.33	8.25	0.1309	-2.2	0.114	1.14	0.43	1.68	7.9	0.21	6.77	6.21	8.30	-4.2	1.15	
1.39	8.7	0.1240	3.0	0.108	1.16	0.46	1.73	7.6	0.23	6.26	5.90	8.17	-4.6	1.38	
1.42	9	0.1651	-7.3	0.144	1.29	0.42	1.85	7.9	0.23	7.78	6.02	7.79	-4.8	1.36	
1.46	9.15	0.0781	33.1	0.068									1.34		
1.52	9.4	0.1152	10.2	0.100	1.28	0.41	1.80	8.1	0.22	5.58	6.34	8.40	-4.9	1.35	
1.60	9.7	0.1191	24.0	0.104		0.41		7.6				8.04	-6.1	1.01	
1.71	10.15	0.0752	26.6	0.065	1.26	0.36	1.68	7.9	0.21	3.89	6.24	8.30	-5.8	1.38	
1.79	10.35	0.0888	1.6	0.077	1.26	0.40	1.74	7.8	0.22	4.45	6.10	8.85	-5.8	1.39	
1.82	10.65	0.1154	0.3	0.100	1.14	0.44	1.68	7.9	0.21	5.97	6.19	8.42	-5.0	1.61	
1.85	10.95	0.1387	11.2	0.121	0.99	0.41	1.52	8.0	0.19	7.94	6.52	8.51	-5.3	1.51	
1.89	11.4	0.1478	-2.2	0.129	1.13	0.41	1.67	7.8	0.21	7.71	6.11	8.49	-5.0	1.72	
1.93	11.85	0.1350	1.8	0.118	1.16	0.39	1.67	7.7	0.22	7.05	6.03	8.60	-4.8	1.69	
2.00	12.55	0.1331	4.2	0.116	1.14	0.39	1.65	7.7	0.21	7.03	6.06	8.22	-5.6	1.25	
2.02	12.7	0.0870	-2.5	0.076	1.19	0.39	1.66	7.9	0.21	4.56	6.24	8.40	-4.9	1.44	
2.06	13.15	0.1451	-11.8	0.126	1.21	0.39	1.73	7.6	0.23	7.30	5.84	8.09	-5.2	1.57	
2.07	13.3	0.1464	-13.7	0.127	1.01	0.43	1.56	7.8	0.20	8.16	6.21	8.11	-4.8	1.71	
2.15	13.65	0.2052	-2.5	0.179	1.03	0.43	1.64	7.7	0.21	10.91	6.07	7.84	-5.4	1.69	
2.20	13.8	0.2568	-7.5	0.224	1.18	0.43	1.84	7.7	0.24	12.15	5.85	7.90	-4.7	1.72	
2.30	14.1	0.2061	-9.4	0.180	1.08	0.44	1.70	7.6	0.22	10.58	5.93	8.63	-4.4	1.73	
2.51	14.7	0.1790	-16.3	0.156	1.17	0.44	1.77	7.4	0.24	8.80	5.64	8.25	-5.0	1.64	
2.62	15.25	0.1681	-10.5	0.146	0.95	0.54	1.64	7.3	0.22	8.93	5.69	8.52	-4.6	1.64	
2.65	15.4	0.1832	-18.9	0.160	0.97	0.42	1.54	7.6	0.20	10.33	6.03	8.94	-3.5	1.70	
2.74	15.85	0.1941	-15.2	0.169	1.10	0.41	1.68	7.2	0.23	10.05	5.52		-3.4	1.58	
2.77	16	0.2271	-20.9	0.198	1.05	0.40	1.65	7.53	0.22	12.00	5.88		-3.5	1.76	
2.80	16.15	0.2233	-13.7	0.194	1.15	0.41	1.75	7.6	0.23	11.10	5.85	8.40	-4.1	1.74	
2.86	16.45	0.1852	-16.4	0.161	1.07	0.40	1.63	7.7	0.21	9.90	6.03	8.10	-4.3	1.59	
2.93	16.8	0.1543	-8.4	0.134	0.99	0.46	1.59	7.3	0.22	8.46	5.71	7.26	-5.4	1.28	
2.99	17.1	0.1395	-5.5	0.122	0.96	0.56	1.65	7.2	0.23	7.38	5.60	7.29	-4.6	1.49	
3.05	17.4	0.2266	-16.2	0.197	0.97	0.41	1.57	7.2	0.22	12.56	5.65	8.60	-3.5	1.90	
3.08	17.55	0.2575	-10.0	0.224	0.96	0.56	1.74	7.1	0.24	12.87	5.39	8.39	-3.7	2.36	
3.11	17.7	0.2243	-12.5	0.195	0.87	0.40	1.47	7.1	0.21	13.28	5.59	7.68	-4.9	1.76	
3.20	18.15	0.2431	19.9	0.212			7.4								
3.22	18.23	0.2076	-8.3	0.181	0.94	0.44	1.56	7.7	0.20	11.61	6.10	7.72	-4.3	1.74	
3.25	18.4	0.1222	-14.5	0.106	0.89	0.40	1.40	7.6	0.18	7.61	6.20	7.90	-5.3	0.785	
3.31	18.7	0.1698	-5.3	0.148	0.92	0.44	1.51	7.0	0.21	9.81	5.51	7.40	-5.1	1.73	
3.40	19.15	0.1866	-4.4	0.162	0.98	0.38	1.52	7.1	0.22	10.66	5.54	8.91	-6.9	0.622	
3.48	19.5	0.2427	0.9	0.211	0.83	0.36	1.40	6.5	0.21	15.09	5.12	7.92	-6.2	1.59	
3.51	19.65	0.2195	3.7	0.191	0.87	0.49	1.56	7.1	0.22	12.28	5.54		-6.8	1.74	
3.60	20.1	0.2160	-7.2	0.188	0.90	0.37	1.47	6.9	0.21	12.83	5.44	8.02	-6.0	1.72	
3.69	20.55	0.2680	0.9	0.233	0.73	0.36	1.33	6.5	0.21	17.55	5.16	8.11	-5.9	1.73	
3.78	21	0.2534	-2.8	0.221	0.82	0.38	1.43	6.9	0.21	15.48	5.47	8.83	-5.9	1.76	
3.81	21.15	0.1211	-11.8	0.105											

Table 2. (continued)

Age (kyr BP)	Depth (mbsf)	CRS (wt %)	$\delta^{34}\text{S}_{\text{CRS}}$ (‰ VCDT)	Fe_{CRS} (wt%)	Fe_{D} (wt %)	Fe_{Ox} (wt %)	Fe_{HR} (wt %)	Fe_{T} (wt %)	$\text{Fe}_{\text{HR}}/\text{Fe}_{\text{T}}$	DOP (%)	Fe_{PR} (wt %)	Al (wt %)	$^{13}\text{C}_{\text{TIC}}$ (‰ VPDB)	TOC (wt %)	$\text{Fe}_{\text{PR}}/\text{Al}$
3.86	21.4	0.2310	-3.4	0.201	0.81	0.50	1.51	6.7	0.22	13.36	5.24	7.80	-6.6	1.67	0.671
3.89	21.55	0.1910	-7.3	0.166	0.99	0.37	1.52	7.0	0.22	10.94	5.52	8.01	-6.2	1.72	0.689
3.92	21.7	0.1400	-6.7	0.122	0.97	0.36	1.46	6.8	0.21	8.38	5.38	8.10	-6.0	1.67	0.664
4.01	22.15	0.1902	-6.8	0.166	0.98	0.49	1.64	6.9	0.24	10.09	5.21	8.12	-7.6	1.76	0.642
4.107	22.65	0.160	-2.7	0.139	0.95	0.37	1.46	6.9	0.21	9.55	5.43	8.19	-6.5		0.663

the studied site via the CO_2 reduction pathway [Whiticar, 1999]. Microbially produced hydrocarbon gases have $\text{C}_1/(\text{C}_2 + \text{C}_3)$ greater than 1000 due to the dominance of methane relative to ethane and propane, while the ratio in thermogenic gases is below 100 due to considerable proportions of ethane and propane [Bernard, 1978]. Acetate, formate, methanol, methylated amines (mono, di, and trimethylamines) and certain

**Figure 5.** (a) Vertical profile of CRS and TOC (wt %) and (b) cross plot of CRS and TOC (wt %).

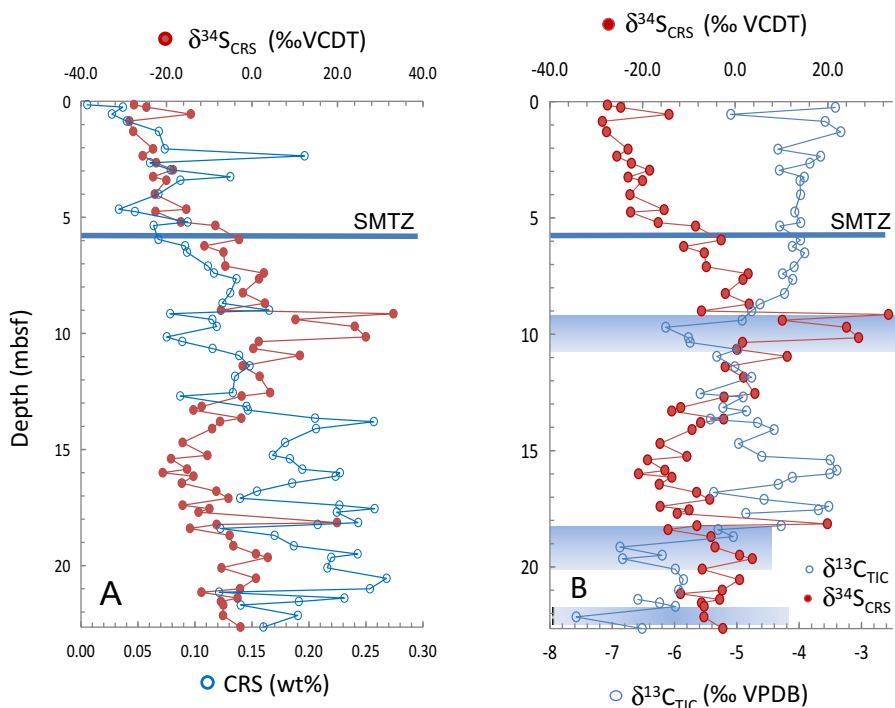


Figure 6. (a) Vertical profile of CRS (wt %) and $\delta^{34}\text{S}_{\text{CRS}}$ (VCDT) and (b) vertical profiles of $\delta^{13}\text{C}_{\text{TIC}}$ and $\delta^{34}\text{S}_{\text{CRS}}$. Blue shade represents the possible paleo-SMTZs.

organic sulfur compounds act as substrates for methanogenesis. The observed ^{13}C depletion of methane may be attributed to the recycling of AOM-derived ^{13}C -depleted DIC by methanogens [Borowski *et al.*, 1997; Hoehler *et al.*, 2000; Pohlman *et al.*, 2008; Holler *et al.*, 2011] and microbially mediated carbon isotope equilibration between methane and carbon dioxide [Yoshinaga *et al.*, 2014]. Other factors which may influence $\delta^{13}\text{C}_{\text{CH}_4}$ values include methanogenic precursors, fractionation factor, and temperature [Alperin *et al.*, 1992; Whiticar, 1999]. The possible contribution of acetate fermentation in methanogenesis is difficult to assess in

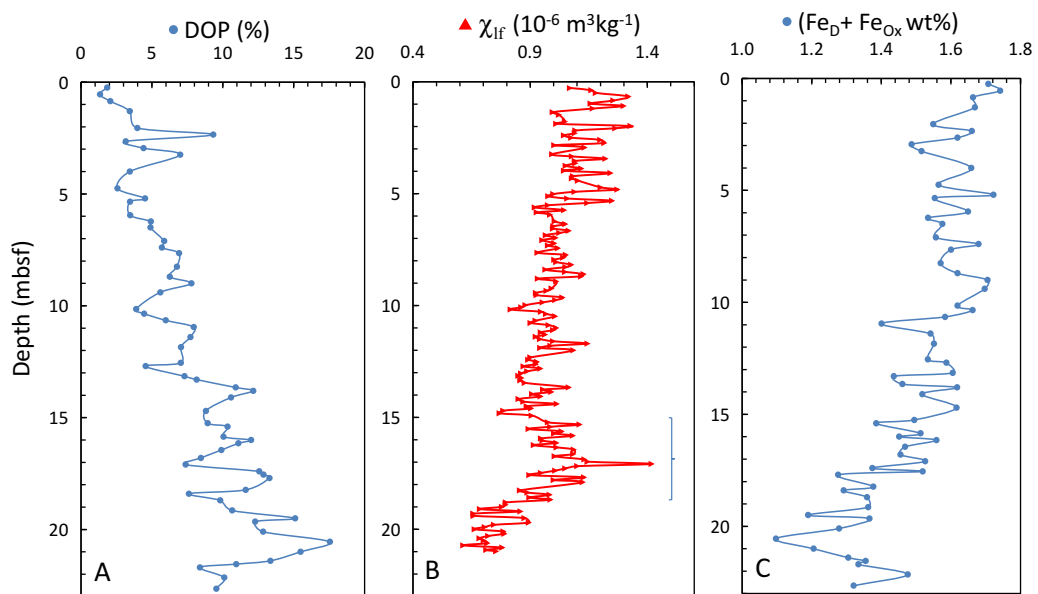


Figure 7. Vertical profiles of (a) Fe_D wt % and (b) DOP values and magnetic susceptibility. The bracket shows the zone of enhanced susceptibility.

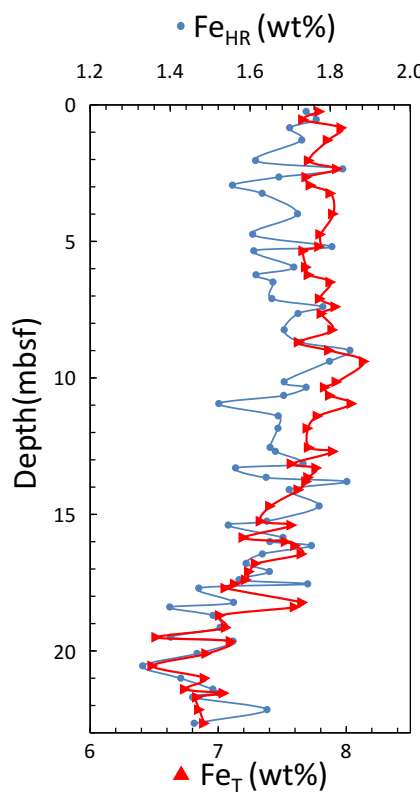


Figure 8. Fe_{HR} and Fe_{T} contents profile.

the absence of δD_{CH_4} , $\delta^{13}\text{C}_{\text{acetate}}$, and acetate concentration measurements [Conrad, 2005]. Approximately 6‰ down core enrichment in carbon isotope ratio of methane observed below SMTZ may be attributed to the continued preferential removal of the isotopically lighter molecules from the carbon pool (CO_2) during methanogenesis resulting in a progressive shift in the residual substrate toward enriched stable carbon isotope ratios following Rayleigh fractionation [Whiticar, 1999]. Mazumdar *et al.* [2012a, 2014b] reported down core (below SMTZ) increase in residual $\delta^{13}\text{C}_{\text{CH}_4}$ values ranging from 3 to 19‰ from K-G and Mahanadi basin cores. Much greater enrichment is expected at greater depths [Paull *et al.*, 2000].

5.2. Sulfate Reduction and Evidence of AOM

The shape of the pore water sulfate concentration profile by bacterial sulfate reduction is controlled by the availability of labile organic matter, diffusive/advective methane flux, and depositional conditions [Niewöhner *et al.*, 1998; Zabel and Schulz, 2001; Hensen *et al.*, 2003; Schmidt *et al.*, 2005; Treude *et al.*, 2005; Kastner *et al.*, 2008]. A linear sulfate profile is commonly attributed to AOM caused by high methane flux [Borowski *et al.*, 1996] from the gas-rich zone underlying our study area [Mazumdar *et al.*, 2012a]. The parabolic TA profile (Figure 3a) across the SMTZ associated with the quasi-linear sulfate concentration trend is typical of AOM [Schmidt *et al.*, 2005; Kastner *et al.*, 2008; Ussler and Paull, 2008]. Vertical diffusion of

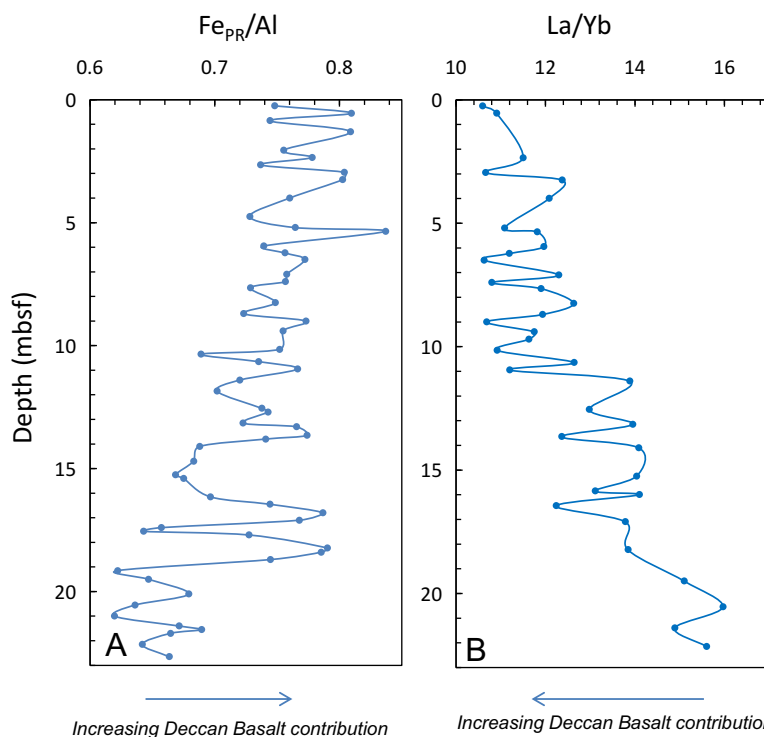


Figure 9. Vertical profiles of (a) $\text{Fe}_{\text{PR}}/\text{Al}$ and (b) La/Yb ratios.

Table 3. La and Yb Concentrations

Depth (mbsf)	La (ppm)	Yb (ppm)	La/Yb
0.25	23.3	2.2	10.6
0.55	25.2	2.31	10.9
2.35	26.1	2.27	11.5
2.95	25.8	2.42	10.7
3.25	26.1	2.11	12.4
4	26.7	2.21	12.1
5.2	24.5	2.21	11.1
5.35	29.3	2.48	11.8
5.95	25.6	2.14	12.0
6.23	24.5	2.19	11.2
6.5	23.7	2.23	10.6
7.1	26.8	2.18	12.3
7.4	25.7	2.38	10.8
7.65	26.3	2.21	11.9
8.25	29.8	2.36	12.6
8.7	28.4	2.38	11.9
9	25	2.34	10.7
9.4	27.6	2.35	11.7
9.7	30	2.58	11.6
10.15	25	2.29	10.9
10.65	27.8	2.2	12.6
10.95	27.1	2.42	11.2
11.4	30.4	2.19	13.9
12.55	29.2	2.25	13.0
13.15	31.8	2.28	13.9
13.65	30.9	2.5	12.4
14.1	30.7	2.18	14.1
15.25	32	2.28	14.0
15.85	29.5	2.25	13.1
16	29.6	2.1	14.1
16.45	27.9	2.28	12.2
17.1	30.6	2.22	13.8
18.23	29.9	2.16	13.8
19.5	37.3	2.47	15.1
20.55	36.4	2.28	16.0
21.4	34.1	2.29	14.9
22.15	33.7	2.16	15.6
23.1	37.2	2.41	15.4

HS^- ($\delta^{34}\text{S}_{\text{HS}}^-$) at the time of crystallization. Since pyritization involves insignificant sulfur isotope fractionation, pyrite isotope ratios represent the sulfur isotope ratio of pore water HS^- [Price and Shieh, 1979]. Various iron bearing minerals which are amenable to pyritization in sediments have a wide range of sulfidization half-lives [Canfield et al., 1992; Raiswell and Canfield, 1998; Poulton et al., 2004]. Sulfidization half-lives for various iron minerals have been estimated based on field [Canfield et al., 1992] and laboratory [Poulton et al., 2004] studies. Sulfidization half-lives for Iron(III) oxide-hydroxide (ferrihydrite, lepidocrocite, and goethite) range from 2.8 h to 63 days. Whereas, contrasting sulfidization half-lives have been estimated for iron-oxides like hematite (31–182 days) and magnetite (72 days to 105 years). Sheet silicates, illmenites, garnet, augite, and amphibole have sulfidization half-lives of $\geq 84,000$ years. A high proportion of highly reactive (low half-lives) iron minerals in the sediment leads to enhanced pyritization close to the sediment-water interface. Early diagenetic pyrite forming close to the sediment-water interface is markedly depleted in ^{34}S . ^{34}S depletion in pyrite recorded at the core top is attributed to early diagenetic pyritization close to the sediment-water interface where the rate of sulfate diffusion into the sediment pore volume exceeds the rate of sulfate consumption [Jørgensen, 1979; Calvert et al., 1996; Schenau et al., 2002]. Subsequent burial (late diagenesis) of sediment leads to sulfidization of residual reactive iron and possibly part of reactive iron with higher half-lives by ^{34}S -enriched HS^- in pore water. The late diagenetic enrichment of ^{34}S in pore water HS^- is attributed to sulfate limitation during progressive bacterial sulfate reduction in the pore waters [Kaplan and Rittenberg, 1964; Jørgensen, 1979; Calvert et al., 1996; Wehrmann et al., 2011]. The bulk sediment CRS concentrations as well the S isotope ratios depend on the relative proportions of pyrite crystallization at the sediment-water interface and during late diagenesis [Mazumdar et al., 2012b]. Sulfate reduction via organoclastic and AOM pathways may be represented by the equations (3) and (4), respectively.

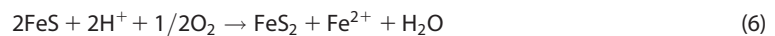
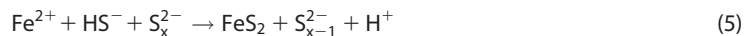
bicarbonate ions produced via focused sulfate reduction at the SMTZ is apparently responsible for the parabolic TA profiles [Ussler and Paull, 2008]. The relative contribution of AOM and organoclastic degradation toward alkalinity may be assessed through the $(\Delta\text{TA} + \Delta\text{Ca} + \Delta\text{Mg})/\Delta\text{SO}_4^{2-}$ ratio of pore waters [Kastner et al., 2008; Solomon et al., 2008; Chen et al., 2010; Burdige and Komada, 2011; Malinverno and Pohlman, 2011; Mazumdar et al., 2014b]. Sulfate reduction solely via organoclastic degradation produces 2 mol of HCO_3^- per mol of SO_4^{2-} reduced (equation 3), while AOM produces 1 mol of HCO_3^- per mol of sulfate reduced (equation 4). In the present study, $(\Delta\text{Ca} + \Delta\text{TA} + \Delta\text{Mg})/\Delta\text{SO}_4^{2-}$ ratios decrease with depth from 2.5 to 1 suggesting increasing influence of AOM on sulfate reduction closer to SMTZ (Figure 4). The intermediate values (1.4–1.5) suggest mixed influence of organoclastic reduction and AOM on pore water sulfate concentration profiles [Kastner et al., 2008].

5.3. Pyritization: Influence of Organoclastic and AOM-Induced Sulfate Reduction

Pyrite concentrations (CRS wt %) and $\delta^{34}\text{S}_{\text{CRS}}$ of marine sediments depend primarily on (a) reactivity of iron amenable for sulfidization, (b) availability of HS^- in the pore waters, (c) sulfur isotope ratio of HS^- , and (d) extent of late diagenetic overprint on early diagenetic pyrite [Mazumdar et al., 2012b]. The second and third factors, in turn depend on sulfate reduction rates either by organoclastic or AOM pathways. The sulfur isotope ratios of pyrite grains depend on the isotope ratio of pore water

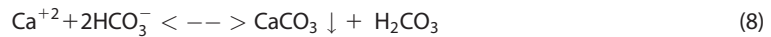


Subsequent pyritization via polysulfide [Rickard, 1975], iron loss [Wilkin and Barnes, 1997], and H₂S pathways [Drobner et al., 1990; Rickard, 1997; Butler et al., 2004] may be represented by equations (5), (6), and (7), respectively,



Figures 5a and 5b show significant positive correlation between the TOC and CRS contents. The positive correlation indicates influence of organoclastic sulfate reduction on sulfidization. The contribution of organoclastic sulfate reduction is also supported by the $(\Delta\text{Ca} + \Delta\text{TA} + \Delta\text{Mg})/\Delta\text{SO}_4^{2-}$ ratios of pore waters (Figure 4). High sedimentation rates during the late Holocene in K-G basin (Figure 2) is the most likely reason for enhanced preservation of labile organic matter amenable to sulfate reducers [Mazumdar et al., 2009, 2012a; Solomon et al., 2014]. Under oxic bottom water conditions, sedimentation rate plays an important role in determining the preservation and pathway of organic matter decomposition [Canfield, 1991]. Hedges and Keil [1995], Hartnett et al. [1998], Hedges et al. [1999], and Gélinas et al. [2001] suggested “oxygen exposure time (OET)” of organic matter as an important factor affecting preservation of labile components. Rapid sedimentation would cut off the oxygen supply below sediment-water interface resulting in amenability of highly labile organic molecules like amino acids and acetates to sulfate reducers.

Highly depleted sulfur isotope ratios of CRS (-24.7 to $-28.7\text{\textperthousand}$) in the top 0.85 mbsf (Figure 6a) suggest a S isotopic fractionation of 46–50‰ relative to the average sea water sulfate sulfur isotope ratio of $\sim 21\text{\textperthousand}$ [Rees et al., 1978]. The reported fractionation is more than the range of sulfur isotopic fractionation (5–46‰) measured for natural environment and laboratory cultures [Canfield and Teske, 1996; Habicht and Canfield, 1996]. The high fractionation observed in our study may be attributed to the disproportionation of sulfur intermediates like S⁰, SO₃²⁻, and S₂O₃²⁻ produced during oxidative part of sulfur cycle [Canfield and Thamdrup, 1994]. Disproportionation may play an important role in early diagenetic sulfidization close to the sediment-water interface due to high burrowing activities leading to the oxidation of HS⁻ [Canfield and Farquhar, 2009]. However, field observations [Wortmann et al., 2001], experimental [Sim et al., 2011], and modeling studies [Brunner and Bernasconi, 2005] suggest significant depletion in ³⁴S and fractionation up to 70‰ may directly be caused by dissimilatory sulfate reduction without disproportionation of sulfur intermediates. The pyrite sulfur isotope profile shows stepwise increase in $\delta^{34}\text{S}$ down to a depth of 10.15 mbsf (Figure 6). The increase in $\delta^{34}\text{S}$ values from -22.6 to $-3\text{\textperthousand}$ within 4.75–6 mbsf (Figure 6) is associated with the present sulfate methane transition zone suggesting possible influence of the AOM on sulfate reduction. A high sulfate reduction rate via AOM pathway [JØrgensen et al., 2004; JØrgensen and Parkes, 2010] may result in rapid sulfate limitation and ³⁴S enrichment of pore water HS⁻. The rise in ³⁴S_{CRS} is attributed to the buildup of isotopically enriched HS⁻ pool (equation (4)) due to vertical methane flux [Borowski et al., 1996]. A sharp rise in $\delta^{34}\text{S}_{\text{SO}_4}$ to $+92\text{\textperthousand}$ corroborates the rapid sulfate limitation pathway (Figure 3c). Very high $\delta^{34}\text{S}_{\text{CRS}}$ values ($+26.6$ to $+33\text{\textperthousand}$; Figure 6b) recorded within the depth zone 9.15–10.15 mbsf possibly suggest remanence of paleo-AOM-induced sulfidization fueled by high methane flux at a paleo-sulfate methane transition zone [Borowski et al., 1996; Wehrmann et al., 2011; Peketi et al., 2012]. However, a low CRS content within this zone suggests low pyritization possibly due to low reactivity of the iron pool or low residual HS⁻ concentrations (Figure 6a). Wang et al. [2008] attributed isotopically extremely enriched pyrite particles ($\delta^{34}\text{S}_{\text{PY}} = \sim 53\text{\textperthousand}$) to the formation of pyrite from isotopically highly enriched sulfate under very low sulfate concentrations. Borowski et al. [1996] attributed enriched sulfide ($\delta^{34}\text{S} = \sim +30\text{\textperthousand}$) to focused consumption of sea water sulfate at the base of the sulfate reduction zone. Paleo-intensification of AOM is also supported by the occurrences of ¹³C-depleted authigenic carbonates within the ³⁴S-enriched zones (Figure 6b). AOM results in the depth-focused sulfate consumption and bicarbonate production at the SMTZ leading to precipitation of Ca-Mg carbonates (equation 8) with depleted carbon isotopic ratios [Ussler and Paul, 2008; Mazumdar et al., 2009; Lim et al., 2011].



The $\delta^{13}\text{C}_{\text{TIC}}$ reported here is partially influenced by the presence of foraminifera with the calcareous test having $\delta^{13}\text{C}$ value ranging from -1 to $+1\text{\textperthousand}$ [Joshi *et al.*, 2014] and pure authigenic carbonates resulting from AOM could have been even more ^{13}C depleted. The $\delta^{34}\text{S}_{\text{CRS}}$ profile shows significant depletion in ^{34}S within the depth zone of 13–16 mbsf. However, high CRS content in this zone suggests dominant pyritization at or close to sediment-water interface. Further down (18–22 mbsf), the ^{34}S enrichment in CRS including a positive $\delta^{34}\text{S}$ spike ($19.9\text{\textperthousand}$ VCDT) at 18.15 mbsf is associated with drop in $\delta^{13}\text{C}_{\text{TIC}}$ values suggest influence of AOM-induced sulfidization and carbonate precipitation. These also indicate record of paleo-SMTZs.

The degree of pyritization (DOP) increases down core with enhanced pyritization pulses (Figure 7b). The opposite relationship between DOP and $\text{Fe}_{\text{D}} + \text{Fe}_{\text{ox}}$ profiles (Figures 7b and 7c) along with down core decrease in magnetic susceptibility suggests dissolution/sulfidization of magnetic minerals [Karlin and Levi, 1983; Canfield and Berner, 1987; Channell and Hawthorne, 1990; Nowaczyk, 2011]. The enhanced magnetic susceptibility within the depth zone (15.32–18.65 mbsf) may be attributed to change in magnetic mineral assemblage (A. Usapkar, *et al.*, manuscript in preparation, 2015). The enhanced DOP pulse is observed within the depth zone of 18–22 mbsf. This is also the zone of highly ^{13}C -depleted TIC and ^{34}S -enriched CRS. The observation may be attributed to availability of HS^- driven by AOM process. The results also suggest that for paleoclimatic application of magnetic susceptibility, DOP analyses should also be taken into consideration.

5.4. Possible Iron Sources

The sediments of the K-G basin are derived from the Archean-Proterozoic peninsular gneissic complexes (APGC) and Deccan basalts [Mazumdar *et al.*, 2014a]. Ferruginous soil covers [Rengasamy *et al.*, 1978; Bhattacharyya *et al.*, 1993; Goulart *et al.*, 1998; Kisakurek *et al.*, 2004; Ollier and Sheth, 2008; Bhattacharyya *et al.*, 2013] developed over these provenances are the sources of reactive iron (Fe_{HR}) to the depositional basin. The overall positive relation between Fe_{T} and Fe_{HR} (Figure 8) suggests the association of Fe_{HR} with detrital particulates supplied primarily as fluvial input. Fe_{HR} in riverine particulates are mostly present as adsorbed nanoparticles of Fe-oxyhydroxides on clay/organic matter [Raiswell, 2011] and detrital Ti-magnetite. Dewangan *et al.* [2013] reported Ti bearing magnetite grains in sediment cores from K-G basin. Ti/Fe ratios range from 0.2 to 0.4 in $<2\text{ }\mu\text{m}$ grains, whereas, larger grains ($>10\text{ }\mu\text{m}$) show Ti/Fi ratio ranging from 0.8 to unity. The larger grains are significantly corroded due to dissolution. The $\text{Fe}_{\text{HR}}/\text{Fe}_{\text{T}}$ ratios are apparently controlled by the runoff and weathering intensity [Canfield, 1997] whereby intense runoff results in relatively greater proportion of hydrated iron oxide phases compared the crystalline iron-oxides [Canfield, 1997; Poulton and Raiswell, 2002]. Very high sedimentation rate possibly indicate high runoff in our study area. The narrow range of $\text{Fe}_{\text{HR}}/\text{Fe}_{\text{T}}$ ratios (Avg. 0.21 ± 0.01) obtained in our study suggest relatively steady flux of reactive iron at the depositional site. The relatively lower $\text{Fe}_{\text{HR}}/\text{Fe}_{\text{T}}$ ratios compared to the global continental margin/deep sea average ($0.28 \pm 0.06/0.25 \pm 0.1$) in our core are attributed to higher Fe_{T} relative to the global average of ($3.69 \pm 0.91/4.29 \pm 0.98$). However, aeolian particulates may also contribute toward reactive iron content [Maher *et al.*, 2010; Raiswell and Canfield, 2012]. The $\text{Fe}_{\text{PR}}/\text{Al}$ ratios (Figure 9a) can be a reliable proxy for iron source differentiation [Lamy *et al.*, 2000, 2001; Dezileau *et al.*, 2007]. The upcore increasing $\text{Fe}_{\text{PR}}/\text{Al}$ ratios suggest relative increase in basalt in sediment flux in K-G basin during the last 4 kyr. Deccan basalts have significantly higher Fe/Al ratios (1.2–1.6) [Pattanayak and Shrivastava, 1999] compared to that of APGC (0.2–0.48) [Naqvi and Rogers, 1987]. Increase in contribution from basalt to the sediment load is further supported by an upcore decrease in La/Yb ratios (Figure 9b) [Dezileau *et al.*, 2004]. The average La/Yb ratio of Deccan basalt is 5.9 ± 1.7 and it varies from 2.6 to 9.4 [Chandrasekharam *et al.*, 1999; Sano *et al.*, 2001; Melluso *et al.*, 2004; Sheth *et al.*, 2004; Bondre *et al.*, 2006] and that of APGC is 47.6 ± 27.3 (7.3–109.7) [Moyen *et al.*, 2003]. Based on magnetic studies of Godavari river sediments, Sangode *et al.* [2007] suggested Deccan provenance as the most significant source of ferrimagnetic iron minerals. Increasing Deccan contribution toward the core top possibly resulted in relatively higher flux ferrimagnetic iron minerals.

6. Conclusions

1. The pore water analyses at the site MD161-13 of K-G basin show very shallow SMTZ (~ 6 mbsf). The $(\Delta\text{TA} + \Delta\text{Ca} + \Delta\text{Mg})/\Delta\text{SO}_4$ ratios suggest that sulfate consumption is a net result of both organoclastic

degradation and AOM. High sedimentation rate during the late Holocene in the K-G basin likely resulted in the preservation of reactive organic matter amenable for sulfate reducers.

2. The CRS concentration profile shows significant correlation with TOC content suggesting influence of organoclastic degradation on pyritization. The net ^{34}S ratio of the pyrite depends on relative contribution of early and late diagenetic pyritization. Pyrite crystallization through sulfidization of reactive iron at the sediment-water interface results in ^{34}S depleted isotope ratios owing to disproportionation of sulfur intermediates. On the other hand, $\delta^{34}\text{S}_{\text{CRS}}$ and $\delta^{13}\text{C}_{\text{TIC}}$ indicate the contribution of AOM-induced sulfate reduction and carbonate precipitation in the sediments. The combined study of $\delta^{34}\text{S}_{\text{CRS}}$ and $\delta^{13}\text{C}_{\text{TIC}}$ helped in understanding the paleo-SMTZs.
3. Fe_{PR} represents primarily the siliciclastic found iron fraction in the sediment. The upcore trend of $\text{Fe}_{\text{PR}}/\text{Al}$ suggests increasing contribution of Deccan basalt in the K-G basin sediments during the last 4 kyr. This interpretation is further supported by the La/Yb ratios.

Acknowledgments

We thank the directors of NIO, NIOT, NCAOR, advisor MOES for supporting this study. The research is funded by MOES. Head oceanography department and in-charge onboard operations of IPEV are thanked for providing onboard technical support and facilities. Sincere thanks to students of Goa University, IIT Kharagpur and project scientists of NIO, NIOT, PRL, and NGRI. Thanks are due to M. Caesar for carrying out XRF analyses at NIO. Sincere thanks to G. N. Naik for providing AAS facility. Thanks are also due to Cheryl, Purnima, and N. Maheshwar for technical assistance. Research fellowship from VNJCT to A. Pekeți is sincerely acknowledged. Requests for original data files may be sent to the corresponding author (maninda@nio.org). Comments from the reviewers are sincerely acknowledged.

References

- Acosta, O. B. G., D. Schleheck, and B. Schink (2014), Acetone utilization by sulfate-reducing bacteria: Draft genome sequence of *Desulfococcus biacutus* and a proteomic survey of acetone-inducible proteins, *BMC Genomics*, 15(1), 584, doi:10.1186/1471-2164-15-584.
- Alperin, M., N. Blair, D. Albert, T. Hoehler, and C. Martens (1992), Factors that control the stable carbon isotopic composition of methane produced in an anoxic marine sediment, *Global Biogeochem. Cycles*, 6, 271–291, doi:10.1029/92GB01650.
- Bastia, R. (2007), *Geologic Settings and Petroleum Systems of India's East Coast Offshore Basins: Concepts and Applications*, 204 pp., Technol. Publ., Dehradun, India.
- Bernard, B. B. (1978), Light hydrocarbons in marine sediments, PhD dissertation, Texas A&M University, Tex.
- Berner, R. A. (1978), Sulfate reduction and the rate of deposition of marine sediments, *Earth Planet. Sci. Lett.*, 37(3), 492–498, doi:10.1016/0012-821X(78)90065-1.
- Berner, R. A. (1980), *Early Diagenesis. A Theoretical Approach*, 256 pp., Princeton Univ. Press, N. J.
- Bhattacharya, T., D. Pal, and S. Deshpande (1993), Genesis and transformation of minerals in the formation of red (Alfisols) and black (Inceptisols and Vertisols) soils on Deccan basalt in the Western Ghats, India, *J. Soil Sci.*, 44(1), 159–171, doi:10.1111/j.1365-2389.1993.tb00442.x.
- Bhattacharyya, T., D. K. Pal, C. Mandal, P. Chandran, S. K. Ray, D. Sarkar, K. Velmourougane, A. Srivastava, G. S. Sidhu, and R. S. Singh (2013), Soils of India: Historical perspective, classification and recent advances, *Curr. Sci.*, 104(10), 1308–1323.
- Biksham, G., and V. Subramanian (1988), Sediment transport of the Godavari River basin and its controlling factors, *J. Hydrol.*, 101(1–4), 275–290, doi:10.1016/0022-1694(88)90040-6.
- Boetius, A., K. Ravenschlag, C. J. Schubert, D. Rickert, F. Widdel, A. Giesecke, R. Amann, B. B. Jørgensen, U. Witte, and O. Pfannkuche (2000), A marine microbial consortium apparently mediating anaerobic oxidation of methane, *Nature*, 407, 623–626, doi:10.1038/35036572.
- Bondre, N. R., W. K. Hart, and H. C. Sheth (2006), Geology and geochemistry of the Sangamner mafic dike swarm, western Deccan volcanic province, India: Implications for regional stratigraphy, *J. Geol.*, 114(2), 155–170, doi:10.1086/499568.
- Borowski, W., C. Paull, and W. Ussler III (1996), Marine pore-water sulfate profiles indicate in situ methane flux from underlying gas hydrate, *Geology*, 24(7), 655–658, doi:10.1130/0091-7613.
- Borowski, W. S., C. K. Paull, and W. Ussler III (1997), Carbon cycling within the upper methanogenic zone of continental rise sediments: An example from the methane-rich sediments overlying the Blake Ridge gas hydrate deposits, *Mar. Chem.*, 57, 299–311, doi:10.1016/S0304-4203(97)00019-4.
- Borowski, W. S., C. K. Paull, and W. Ussler III (1999), Global and local variations of interstitial sulfate gradients in deep-water, continental margin sediments: Sensitivity to underlying methane and gas hydrates, *Mar. Geol.*, 159(1–4), 131–154, doi:10.1016/S0025-3227(99)00004-3.
- Bowles, M. W., J. M. Mogollon, S. Kasten, M. Zabel, and K.-U. Hinrichs (2014), Global rates of marine sulfate reduction and implications for sub-sea-floor metabolic activities, *Science*, 344(6186), 889–891, doi:10.1126/science.1249213.
- Bradley, A. S., W. D. Leavitt, and D. T. Johnston (2011), Revisiting the dissimilatory sulfate reduction pathway, *Geobiology*, 9(5), 446–457, doi:10.1111/j.1472-4669.2011.00292.x.
- Brüchert, V. (1998), Early diagenesis of sulfur in estuarine sediments: The role of sedimentary humic and fulvic acids, *Geochim. Cosmochim. Acta*, 62(9), 1567–1586, doi:10.1016/S0016-7037(98)00089-1.
- Brüchert, V. (2004), Physiological and ecological aspects of sulfur isotope fractionation during bacterial sulfate reduction, in *Sulfur Biogeochemistry—Past and Present: GSA Special Paper*, vol. 379, edited by J. Amend, K. Edwards, and T. Lyons, pp. 1–16, Geol. Soc. of Am., Boulder, Colo., doi:10.1130/0-8137-2379-5.1.
- Brüchert, V., and L. M. Pratt (1996), Contemporaneous early diagenetic formation of organic and inorganic sulfur in estuarine sediments from St. Andrew Bay, Florida, USA, *Geochim. Cosmochim. Acta*, 60(13), 2325–2332, doi:10.1016/0016-7037(96)00087-7.
- Brunner, B., and S. M. Bernasconi (2005), A revised isotope fractionation model for dissimilatory sulfate reduction in sulfate reducing bacteria, *Geochim. Cosmochim. Acta*, 69(20), 4759–4771, doi:10.1016/j.gca.2005.04.015.
- Burdige, D. J., and T. Komada (2011), Anaerobic oxidation of methane and the stoichiometry of remineralization processes in continental margin sediments, *Limnol. Oceanogr.*, 56(5), 1781–1798, doi:10.4319/lo.2011.56.5.1781.
- Butler, I. B., M. E. Bottcher, D. Rickard, and A. Oldroyd (2004), Sulfur isotope partitioning during experimental formation of pyrite via the polysulfide and hydrogen sulfide pathways: Implications for the interpretation of sedimentary and hydrothermal pyrite isotope records, *Earth Planet. Sci. Lett.*, 228(3–4), 495–509, doi:10.1016/j.epsl.2004.10.005.
- Calvert, S., H. Thode, D. Yeung, and R. Karlin (1996), A stable isotope study of pyrite formation in the Late Pleistocene and Holocene sediments of the Black Sea, *Geochim. Cosmochim. Acta*, 60(7), 1261–1270, doi:10.1016/0016-7037(96)00020-8.
- Canfield, D. E. (1989a), Sulfate reduction and oxic respiration in marine sediments: Implications for organic carbon preservation in euxinic environments, *Deep Sea Res., Part A*, 36(1), 121–138, doi:10.1016/0198-0149(89)90022-8.
- Canfield, D. E. (1989b), Reactive iron in marine sediments, *Geochim. Cosmochim. Acta*, 53(3), 619–632, doi:10.1016/0016-7037(89)90005-7.

- Canfield, D. E. (1991), Sulfate reduction in deep-sea sediments, *Am. J. Sci.*, 291(2), 177–188, doi:10.2475/ajs.291.2.177.
- Canfield, D. E. (1997), The geochemistry of river particulates from the continental USA: Major elements, *Geochim. Cosmochim. Acta*, 61, 3349–3365, doi:10.1016/S0016-7037(97)00172-5.
- Canfield, D. E. (2001), Biogeochemistry of sulfur isotopes, *Rev. Mineral. Geochem.*, 43(1), 607–636, doi:10.2138/gsmg.43.1.607.
- Canfield, D. E., and R. A. Berner (1987), Dissolution and pyritization of magnetite in anoxic marine sediments, *Geochim. Cosmochim. Acta*, 51, 645–659, doi:10.1016/0016-7037(87)90076-7.
- Canfield, D. E., and J. Farquhar (2009), Animal evolution, bioturbation, and the sulfate concentration of the oceans, *Proc. Natl. Acad. Sci. U. S. A.*, 106(20), 8123–8127, doi:10.1073/pnas.0902037106.
- Canfield, D. E., and A. Teske (1996), Late proterozoic rise in atmospheric oxygen concentration inferred from phylogenetic and sulphur-isotope studies, *Nature*, 382, 127–132, doi:10.1038/382127a0.
- Canfield, D. E., and B. Thamdrup (1994), The production of ^{34}S -depleted sulfide during bacterial disproportionation of elemental sulfur, *Science*, 266(5193), 1973–1975, doi:10.1126/science.11540246.
- Canfield, D. E., R. Raiswell, J. T. Westrich, C. M. Reaves, and R. A. Berner (1986), The use of chromium reduction in the analysis of reduced inorganic sulphur in sediments and shales, *Chem. Geol.*, 54, 149–155, doi:10.1016/0009-2541(86)90078-1.
- Canfield, D. E., R. Raiswell, and S. Bottrell (1992), The reactivity of sedimentary iron minerals toward sulfide, *Am. J. Sci.*, 292, 659–683, doi:10.2475/ajs.292.9.659.
- Canfield, D. E., K. Erik, and T. Bo (2005), The sulfur cycle, *Adv. Mar. Biol.*, 48, 313–381.
- Canfield, D. E., C. A. Olesen, and R. P. Cox (2006), Temperature and its control of isotope fractionation by a sulfate-reducing bacterium, *Geochim. Cosmochim. Acta*, 70, 548–561, doi:10.1016/j.gca.2005.10.028.
- Chandrasekharam, D., J. J. Mahoney, H. C. Sheth, and R. A. Duncan (1999), Elemental and Nd-Sr-Pb isotope geochemistry of flows and dikes from the Tapi rift, Deccan flood basalt province, India, *J. Volcanol. Geotherm. Res.*, 93(1), 111–123, doi:10.1016/S0377-0273(99)00081-5.
- Channell, J. E. T., and T. Hawthorne (1990), Progressive dissolution of titanomagnetites at ODP Site 653 (Tyrrhenian Sea), *Earth Planet. Sci. Lett.*, 96, 469–480, doi:10.1016/0012-821X(90)90021-O.
- Chanton, J., C. Martens, and M. Goldhaber (1987), Biogeochemical cycling in an organic-rich coastal marine basin. 8. A sulfur isotopic budget balanced by differential diffusion across the sediment-water interface, *Geochim. Cosmochim. Acta*, 51(5), 1201–1208, doi:10.1016/0016-7037(87)90212-2.
- Chen, Y., W. Ussler III, H. Hafliðason, A. Lepland, L. Rise, M. Hovland, and B. O. Hjelstuen (2010), Sources of methane inferred from pore-water $\delta^{13}\text{C}$ of dissolved inorganic carbon in Pockmark G11, offshore Mid-Norway, *Chem. Geol.*, 275(3), 127–138, doi:10.1016/j.chemgeo.2010.04.013.
- Chen, Y., J. Zhao, L. Yin, J. Chen, and D. Yuan (2013), Quantification, morphology and source of humic acid, kerogen and black carbon in offshore marine sediments from Xiamen Gulf, China, *J. Environ. Sci.*, 25(2), 287–294, doi:10.1016/S1001-0742(12)60043-6.
- Claypool, G. (2004), Ventilation of marine sediments indicated by depth profiles of pore water sulfate and $\delta^{34}\text{S}$, *Spec. Publ. Geochim. Soc.*, 9, 59–65, doi:10.1016/S1873-9881(04)80007-5.
- Conrad, R. (2005), Quantification of methanogenic pathways using stable carbon isotopic signatures: A review and a proposal, *Org. Geochem.*, 36(5), 739–752, doi:10.1016/j.orggeochem.2004.09.006.
- Cornwell, J. C., and J. W. Morse (1987), The characterization of iron-sulfide minerals in anoxic marine sediments, *Mar. Chem.*, 22, 193–206, doi:10.1016/0304-4203(87)90008-9.
- Detmers, J., V. Bruchert, K. S. Habicht, and J. Kuever (2001), Diversity of sulfur isotope fractionations by sulfate-reducing prokaryotes, *Appl. Environ. Microbiol.*, 67(2), 888–894, doi:10.1016/0304-4203(87)90008-9.
- Dewangan, P., T. Ramprasad, M. Ramana, A. Mazumdar, and M. Desa (2010), Seabed morphology and gas venting features in the continental slope region of Krishna-Godavari basin, Bay of Bengal: Implications in gas-hydrate exploration, *Mar. Petrol. Geol.*, 27, 1628–1641, doi:10.1016/j.marpetgeo.2010.03.015.
- Dewangan, P., N. Basavaiah, F. K. Badesab, A. Usapkari, and A. Mazumdar (2013), Diagenesis of magnetic minerals in a gas hydrate/cold seep environment off the Krishna-Godavari basin, Bay of Bengal, *Mar. Geol.*, 340, 57–70, doi:10.1016/j.margeo.2013.04.016.
- Dezileau, L., O. Ulloa, D. Hebbeln, F. Lamy, J. L. Reyss, and M. Fontugne (2004), Iron control of past productivity in the coastal upwelling system off the Atacama Desert, Chile, *Paleoceanography*, 19, PA3012, doi:10.1029/2004PA001006.
- Dezileau, L., C. Pizarro, and M. A. Rubio (2007), Sequential extraction of iron in marine sediments from the Chilean continental margin, *Mar. Geol.*, 241, 111–116, doi:10.1016/j.margeo.2007.03.006.
- Drobner, E., H. Huber, G. Wächtershäuser, D. Rose, and K. Stetter (1990), Pyrite formation linked with hydrogen evolution under anaerobic conditions, *Nature*, 346, 742–744, doi:10.1038/346742a0.
- Eckert, T., B. Brunner, E. A. Edwards, and U. G. Wortmann (2011), Microbially mediated re-oxidation of sulfide during dissimilatory sulfate reduction by *Desulfovibacter latus*, *Geochim. Cosmochim. Acta*, 75(12), 3469–3485, doi:10.1016/j.gca.2011.03.034.
- Fairbanks, R. G., R. A. Mortlock, T. C. Chiu, L. Cao, A. Kaplan, T. P. Guilderson, T. W. Fairbanks, A. L. Bloom, P. M. Grootes, and M. J. Nadeau (2005), Radiocarbon calibration curve spanning 0 to 50,000 years BP based on paired $^{230}\text{Th}/^{234}\text{U}/^{238}\text{U}$ and ^{14}C dates on pristine corals, *Quat. Sci. Rev.*, 24(16–17), 1781–1796, doi:10.1016/j.quascirev.2005.04.007.
- Gélinas, Y., J. Baldock, and J. Hedges (2001), Organic carbon composition of marine sediments: Effect of oxygen exposure on oil generation potential, *Science*, 294(5540), 145–148, doi:10.1126/science.1062363.
- Gieskes, J., T. Gamo, and H. Brumsack (1991), Chemical methods for interstitial water analysis aboard JOIDES Resolution, *Tech. Note 15*, pp. 3–59, Ocean Drill. Program, College Station, Tex.
- Goldhaber, M. (2003), Sulfur-rich sediments, *Treatise Geochem.*, 7, 257–288, doi:10.1016/B0-08-043751-6/07139-5.
- Goldhaber, M., and I. Kaplan (1975), Controls and consequences of sulfate reduction rates in recent marine sediments, *Soil Sci.*, 119(1), 42–55, doi:10.1097/00010694-197501000-00008.
- Goulart, A. T., J. D. Fabris, M. F. Jesus Filho, J. M. D. De Coey, G. M. Da Costa, and E. De Grave (1998), Iron oxides in a soil developed from basalt, *Clays Clay Miner.*, 46, 369–378, doi:10.1146/CCMN.1998.0460402.
- Gupta, S. (2006), Basin architecture and petroleum system of Krishna Godavari Basin, east coast of India, *Leading Edge*, 25(7), 830–837, doi:10.1190/1.2221360.
- Habicht, K. S., and D. E. Canfield (1996), Sulphur isotope fractionation in modern microbial mats and the evolution of the sulphur cycle, *Nature*, 382, 342–343, doi:10.1038/382342a0.
- Hansen, M. H., K. Ingvorsen, and B. B. Jørgensen (1978), Mechanisms of hydrogen sulfide release from coastal marine sediments to the atmosphere, *Limnol. Oceanogr.*, 23(1), 68–76, doi:10.4319/lo.1978.23.1.0068.
- Harrison, A. G., and H. G. Thode (1958), Mechanism of the bacterial reduction of sulfate from isotopic fractionation studies, *Trans. Farad. Soc.*, 54, 84–92, doi:10.1039/tf9585400084.

- Hartnett, H. E., R. G. Keil, J. I. Hedges, and A. H. Devol (1998), Influence of oxygen exposure time on organic carbon preservation in continental margin sediments, *Nature*, 391(6667), 572–575, doi:10.1038/35351.
- Hedges, J., and R. Keil (1995), Sedimentary organic matter preservation: An assessment and speculative synthesis, *Mar. Chem.*, 49(2–3), 81–115, doi:10.1016/0304-4203(95)00008-F.
- Hedges, J. I., F. S. Hu, A. H. Devol, H. E. Hartnett, E. Tsamakis, and R. G. Keil (1999), Sedimentary organic matter preservation: A test for selective degradation under oxic conditions, *Am. J. Sci.*, 299(7–9), 529–555, doi:10.2475/ajs.299.7-9.529.
- Hensen, C., M. Zabel, K. Pfeifer, T. Schwenk, S. Kasten, N. Riedinger, H. Schulz, and A. Boetius (2003), Control of sulfate pore-water profiles by sedimentary events and the significance of anaerobic oxidation of methane for the burial of sulfur in marine sediments, *Geochim. Cosmochim. Acta*, 67(14), 2631–2647, doi:10.1016/S0016-7037(00)00199-6.
- Hoehler, T., W. Borowski, M. Alperin, N. Rodriguez, and C. Paull (2000), Model, stable isotope and radiotracer characterization of anaerobic methane oxidation in gas hydrates bearing sediments of the Blake ridge, in *Proceedings of the Ocean Drilling Program, Scientific Results*, vol. 164, edited by C. K. Paull et al., pp. 79–85, Ocean Drill. Program, College Station, Tex.
- Holler, T., G. Wegener, H. Niemann, C. Deusner, and T. G. Ferdelman (2011), Carbon and sulfur back flux during anaerobic microbial oxidation of methane and coupled sulfate reduction, *Proc. Natl. Acad. Sci. U. S. A.*, 108, E1484–E1490, doi:10.1073/pnas.1106032108.
- Holmkvist, L., A. Kamshny, V. Bruchert, T. G. Ferdelman, and B. B. Jørgensen (2014), Sulfdization of lacustrine glacial clay upon Holocene marine transgression Arkona Basin, Baltic Sea, *Geochim. Cosmochim. Acta*, 142, 75–94, doi:10.1016/j.gca.2014.07.030.
- Iversen, N., and B. B. Jørgensen (1993), Diffusion coefficients of sulfate and methane in marine sediments: Influence of porosity, *Geochim. Cosmochim. Acta*, 57(3), 571–578, doi:10.1016/0016-7037(93)90368-7.
- Jørgensen, B. (1979), A theoretical model of the stable sulfur isotope distribution in marine sediments, *Geochim. Cosmochim. Acta*, 43(3), 363–374, doi:10.1016/0016-7037(79)90201-1.
- Jørgensen, B. (1982), Mineralization of organic matter in the sea bed—The role of sulphate reduction, *Nature*, 296, 643–645, doi:10.1038/296643a0.
- Jørgensen, B., and S. Kasten (2006), Sulfur cycling and methane oxidation, in *Marine Geochemistry*, edited by H. D. Schulz and M. Zabel, pp. 263–310, Springer, Heidelberg, Germany, doi:10.1007/3-540-32144-6_8.
- Jørgensen, B. B., and R. J. Parkes (2010), Role of sulfate reduction and methane production by organic carbon degradation in eutrophic fjord sediments (Limfjorden, Denmark), *Limnol. Oceanogr.*, 55, 1338–1352, doi:10.4319/lo.2010.55.3.1338.
- Jørgensen, B., M. Böttcher, H. Lüschen, L. Neretin, and I. Volkov (2004), Anaerobic methane oxidation and a deep H₂S sink generate isotopically heavy sulfides in Black Sea sediments, *Geochim. Cosmochim. Acta*, 68(9), 2095–2118, doi:10.1016/j.gca.2003.07.017.
- Joshi, R. K., A. Mazumdar, A. Peketi, P. B. Ramamurtty, B. G. Naik, M. Kocherla, M. Ann Carvalho, P. Mahalakshmi, P. Dewangan, and M. V. Ramana (2014), Gas hydrate destabilization and methane release events in the Krishna-Godavari basin, Bay of Bengal, *Mar. Petrol. Geol.*, 58, 476–489, doi:10.1016/j.marpetgeo.2014.08.013.
- Kaplan, I., and S. Rittenberg (1964), Microbial fractionation of sulfur isotopes, *J. Gen. Microbiol.*, 34, 195–212, doi:10.1099/00221287-34-2-195.
- Karlin, R., and S. Levi (1983), Diagenesis of magnetic minerals in recent haemipelagic sediments, *Nature*, 303(5915), 327–330, doi:10.1038/303327a0.
- Kasten, S., and B. B. Jørgensen (2000), Sulfate reduction in marine sediments, in *Marine Geochemistry*, edited by H. D. Schulz and M. Zabel, pp. 263–282, Springer, Heidelberg.
- Kastner, M., G. Claypool, and G. Robertson (2008), Geochemical constraints on the origin of the pore fluids and gas hydrate distribution at Atwater Valley and Keathley Canyon, northern Gulf of Mexico, *Mar. Petrol. Geol.*, 25(9), 860–872, doi:10.1016/j.marpetgeo.2008.01.022.
- Kisakurek, B., M. Widdowson, and R. H. James (2004), Behavior of Li isotopes during continental weathering: The Bidar laterite profile, India, *Chem. Geol.*, 212(1), 27–44, doi:10.1016/j.chemgeo.2004.08.027.
- Knittel, K., and A. Boetius (2009), Anaerobic oxidation of methane: Progress with an unknown process, *Annu. Rev. Microbiol.*, 63, 311–334, doi:10.1146/annurev.micro.61.080706.093130.
- Kristensen, E. (2000), Organic matter diagenesis at the oxic/anoxic interface in coastal marine sediments, with emphasis on the role of burrowing animals, *Hydrobiologia*, 426(1), 1–24, doi:10.1023/A:1003980226194.
- Kump, L., and R. Garrels (1986), Modeling atmospheric O₂ in the global sedimentary redox cycle, *Am. J. Sci.*, 286(5), 337–360, doi:10.2475/aj.286.5.337.
- Lamy, F., J. Klump, D. Hebbeln, and G. Wefer, (2000), Late quaternary rapid climate change in northern Chile, *Terra Nova*, 12, 8–13, doi:10.1046/j.1365-3121.2000.00265.x.
- Lamy, F., D. Hebbeln, U. Röhl, and G. Wefer (2001), Holocene rainfall variability in southern Chile: A marine record of latitudinal shifts of the Southern Westerlies, *Earth Planet. Sci. Lett.*, 185, 369–382, doi:10.1016/S0012-821X(00)00381-2.
- Li, Y. H., and S. Gregory (1974), Diffusion of ions in sea water and in deep-sea sediments, *Geochim. Cosmochim. Acta*, 38(5), 703–714, doi:10.1016/0016-7037(74)90145-8.
- Lim, Y. C., S. Lin, T. F. Yang, Y.-G. Chen, and C. S. Lau (2011), Variations of methane induced pyrite formation in the accretionary wedge sediments offshore southwestern Taiwan, *Mar. Petrol. Geol.*, 28, 1829–1837, doi:10.1016/j.marpetgeo.2011.04.004.
- Lloyd, R. (1968), Oxygen isotope behavior in the sulfate-water system, *J. Geophys. Res.*, 73(18), 6099–6110, doi:10.1029/JB073i018p06099.
- Madigan, M., J. Martinko, and J. Parker (2000), *Biology of Microorganisms*, Prentice Hall, University of Michigan.
- Maher, B. A., J. M. Prospero, D. Mackie, D. Gaiero, P. P. Hesse, and Y. Balkanski (2010), Global connections between aeolian dust, climate and ocean biogeochemistry at the present day and at the last glacial maximum, *Earth Sci. Rev.*, 99(1), 61–97, doi:10.1080/08120099.2014.898698.
- Malinverno, A., and J. W. Pohlman (2011), Modeling sulfate reduction in methane hydrate-bearing continental margin sediments: Does a sulfate-methane transition require anaerobic oxidation of methane?, *Geochim. Geophys. Geosyst.*, 12, Q07006, doi:10.1029/2011GC003501.
- Mazumdar, A., P. Dewangan, H. M. João, A. Peketi, V. Khosla, M. Kocherla, F. K. Badesab, R. K. Joshi, P. Roxanne, and P. B. Ramamurtty (2009), Evidence of paleo-cold seep activity from the Bay of Bengal, offshore India, *Geochim. Geophys. Geosyst.*, 10, Q06005, doi:10.1029/2008GC002337.
- Mazumdar, A., H. M. Joao, A. Peketi, P. Dewangan, M. Kocherla, R. K. Joshi, and T. Ramprasad (2012a), Geochemical and geological constraints on the composition of marine sediment pore fluid: Possible link to gas hydrate deposits, *Mar. Petrol. Geol.*, 38, 35–52, doi:10.1016/j.marpetgeo.2014.08.013.
- Mazumdar, A., A. Peketi, H. Joao, P. Dewangan, D. V. Borole, and M. Kocherla (2012b), Sulfdization in a shallow coastal depositional setting: Diagenetic and palaeoclimatic implications, *Chem. Geol.*, 322, 68–78, doi:10.1016/j.chemgeo.2012.06.005.
- Mazumdar, A., M. Kocherla, M. Ann Carvalho, A. Peketi, R. K. Joshi, P. Mahalakshmi, H. M. Joao, and R. Jisha (2014a), Geochemical characterization of the Krishna-Godavari and Mahanadi offshore basin (Bay of Bengal) sediments: A comparative study of provenance, *Mar. Petrol. Geol.*, 60, 18–33, doi:10.1016/j.marpetgeo.2014.08.013.

- Mazumdar, A., A. Peketi, H. M. Joao, P. Dewangan, and T. Ramprasad (2014b), Pore-water chemistry of sediment cores off Mahanadi Basin, Bay of Bengal: Possible link to deep seated methane hydrate deposit, *Mar. Petrol. Geol.*, 49, 162–175, doi:10.1016/j.marpetgeo.2013.10.011.
- McKeague, J. A., and J. H. Day (1966), Dithionite-and oxalate-extractable Fe and Al as aids in differentiating various classes of soils, *Can. J. Soil Sci.*, 46(1), 13–22, doi:10.4141/cjss66-003.
- Megonigal, J. P., M. E. Hines, and P. T. Visscher (2003), Anaerobic metabolism: linkages to trace gases and aerobic processes, *Treatise Geochim.*, 8, 317–424, doi:10.1016/B0-08-043751-6/08132-9.
- Mehra, O., and M. Jackson (1960), Iron oxide removal from soils and clays by a dithionite-citrate system buffered with sodium bicarbonate, *Clays Clay Miner.*, 7, 317–327, doi:10.1346/CCMN.1958.0070122.
- Meister, P., B. Liu, T. G. Ferdelman, B. B. Jørgensen, and A. Khalili (2013), Control of sulphate and methane distributions in marine sediments by organic matter reactivity, *Geochim. Cosmochim. Acta*, 104, 183–193, doi:10.1016/j.gca.2012.11.011.
- Melluso, L., M. Barbieri, and L. Beccaluva, (2004), Chemical evolution, petrogenesis, and regional chemical correlations of the flood basalt sequence in the central Deccan Traps, India, *J. Earth Syst. Sci.*, 113(4), 587–603, doi:10.1016/j.marpetgeo.2014.09.005.
- Milucka, J., T. G. Ferdelman, L. Polerecky, D. Franzke, and G. Wegener (2012), Zero-valent sulphur is a key intermediate in marine methane oxidation, *Nature*, 491, 541–546, doi:10.1038/nature11656.
- Moyen, J. F., H. Martin, M. Jayananda, and B. Auvray (2003), Late Archaean granites: A typology based on the Dharwar Craton (India), *Precambrian Res.*, 127(1), 103–123, doi:10.1016/S0301-9268(03)00183-9.
- Naqvi, S. M., and J. J. W. Rogers (1987), *Precambrian Geology of India*, 223 pp., Oxford Univ. Press, University of California.
- Niewöhner, C., C. Hensen, S. Kasten, M. Zabel, and H. Schulz (1998), Deep sulfate reduction completely mediated by anaerobic methane oxidation in sediments of the upwelling area off Namibia, *Geochim. Cosmochim. Acta*, 62(3), 455–464, doi:10.1016/S0016-7037(98)00055-6.
- Nowaczyk, N. R. (2011), Dissolution of titanomagnetite and sulphidization in sediments from Lake Kinneret, Israel, *Geophys. J. Int.*, 187, 34–44, doi:10.1111/j.1365-246X.2011.05120.x.
- Ollier, C. D., and H. C. Sheth (2008), The High Deccan duricrusts of India and their significance for the 'laterite' issue, *J. Earth Syst. Sci.*, 117(5), 537–551, doi:10.1007/s12040-008-0051-9.
- Orphan, V. J., C. H. House, K. U. Hinrichs, K. D. McKeegan, and E. F. DeLong (2001), Methane-consuming archaea revealed by directly coupled isotopic and phylogenetic analysis, *Science*, 293, 484–487, doi:10.1126/science.1061338.
- Pattanayak, S. K., and J. P. Srivastava (1999), Petrography and major-oxide geochemistry of Basalts from the eastern Deccan Volcanic province, India, *Geol. Soc. India Mem.*, 43, 233–270.
- Paull, C. K., T. D. Lorenson, W. S. Borowski, W. Ussler III, K. Olsen, and N. M. Rodriguez (2000), Isotopic composition of CH₄, CO₂ species, and sedimentary organic matter within samples from the Blake Ridge: Gas source implications, in *Proceedings of the Ocean Drilling Program, Scientific Results*, vol. 164, edited by C. K. Paull et al., 67 pp., A&M Texas University, Tex.
- Peketi, A., A. Mazumdar, R. Joshi, D. Patil, P. Srinivas, and A. Dayal (2012), Tracing the paleo sulfate-methane transition zones and H₂S seepage events in marine sediments: An application of CS-Mo systematics, *Geochim. Geophys. Geosyst.*, 13, Q10007, doi:10.1029/2012GC004288.
- Pohlman, J. W., C. Ruppel, D. R. Hutchinson, and R. B. Coffin (2008), Assessing sulfate reduction and methane cycling in a high salinity pore water system in the northern Gulf of Mexico, *Mar. Petrol. Geol.*, 25, 942–951, doi:10.1016/j.marpetgeo.2008.01.016.
- Poulton, S. W. and D. E. Canfield (2005), Development of a sequential extraction procedure for iron: Implications for iron partitioning in continentally derived particulates, *Chem. Geol.*, 214, 209–221, doi:10.1016/j.chemgeo.2004.09.003.
- Poulton, S. W., and R. Raiswell (2002), The low-temperature geochemical cycle of iron: From continental fluxes to marine sediment deposition, *Am. J. Sci.*, 302, 774–805, doi:10.2475/ajs.302.9.774.
- Poulton, S. W., M. Krom, and R. Raiswell (2004), A revised scheme for the reactivity of iron (oxyhydr)oxide minerals towards dissolved sulfide, *Geochim. Cosmochim. Acta*, 68(18), 3703–3715, doi:10.1016/j.gca.2004.03.012.
- Prabhakar, K., and P. Zutshi (1993), Evolution of southern part of Indian east coast basins, *Geol. Soc. India*, 41, 215–215, doi:10.1007/s12594-009-0081-1.
- Price, F., and Y. Shieh (1979), Fractionation of sulfur isotopes during laboratory synthesis of pyrite at low temperatures, *Chem. Geol.*, 27(3), 245–253, doi:10.1016/0009-2541(79)90042-1.
- Raiswell, R. (1997), A geochemical framework for the application of stable sulphur isotopes to fossil pyritization, *J. Geol. Soc.*, 154, 343–356, doi:10.1144/gsjgs.154.2.0243.
- Raiswell, R. (2011), Iron transport from the continents to the open ocean: The aging-rejuvenation cycle, *Elements*, 7(2), 101–106, doi:10.2113/gselements.7.2.101.
- Raiswell, R., and D. E. Canfield (1998), Sources of iron for pyrite formation in marine sediments, *Am. J. Sci.*, 298(3), 219–245, doi:10.2475/ajs.298.3.219.
- Raiswell, R., and D. E. Canfield (2012), The iron biogeochemical cycle past and present, *Geochem. Perspect.*, 1, 1–217, doi:10.7185/geochempersp.1.1.
- Ramana, M., T. Ramprasad, and M. Desa (2001), Seafloor spreading magnetic anomalies in the Enderby Basin, East Antarctica, *Earth Planet. Sci. Lett.*, 191(3–4), 241–255, doi:10.1016/S0012-821X(01)00413-7.
- Ramesh, R., and V. Subramanian (1988), Temporal, spatial and size variation in the sediment transport in the Krishna River basin, India, *J. Hydrol.*, 98(1–2), 53–65, doi:10.1016/0022-1694(88)90205-3.
- Rao, G. (2001), Sedimentation, stratigraphy, and petroleum potential of Krishna-Godavari basin, East Coast of India, *AAPG Bull.*, 85(9), 1623–1643.
- Rao, G., and K. Mani (1993), A study on generation of abnormal pressures in Krishna Godavari basin, India, *Indian J. Petrol. Geol.*, 2(1), 20–30.
- Reeburgh, W. S. (2007), Oceanic methane biogeochemistry, *Chem. Rev.*, 107(2), 486–513, doi:10.1021/cr050362v.
- Rees, C., W. Jenkins, and J. Monster (1978), The sulphur isotopic composition of ocean water sulphate, *Geochim. Cosmochim. Acta*, 42(4), 377–381, doi:10.1016/0016-7037(78)90268-5.
- Rengasamy, P., V. A. K. Sarma, R. S. Murthy, and G. K. Murti (1978), Mineralogy, genesis and classification of ferruginous soils of the eastern Mysore Plateau, India, *J. Soil Sci.*, 29(3), 431–445, doi:10.1111/j.1365-2389.1978.tb00792.x.
- Rickard, D. (1975), Kinetics and mechanism of pyrite formation at low temperatures, *Am. J. Sci.*, 275(6), 636–652, doi:10.2475/ajs.275.6.636.
- Rickard, D. (1997), Kinetics of pyrite formation by the H₂S oxidation of iron (II) monosulfide in aqueous solutions between 25 and 125°C: The rate equation, *Geochim. Cosmochim. Acta*, 61(1), 115–134, doi:10.1016/S0016-7037(96)00321-3.
- Roychoudhury, A. N., J. E. Kostka, and P. Van Cappellen (2003), Pyritization: A palaeoenvironmental and redox proxy reevaluated, *Estuarine Coastal Shelf Sci.*, 57(5–6), 1183–1193, doi:10.1016/S0272-7714(03)00058-1.

- Sangode, S. J., R. Sinha, B. Phartiyal, O. S. Chauhan, and R. K. Mazari (2007), Environmental magnetic studies on some quaternary sediments of varied depositional settings in the Indian sub-continent, *Quat. Int.*, 159, 102–118, doi:10.1016/j.quaint.2006.08.015.
- Sano, T., T. Fujii, S. S. Deshmukh, T. Fukuoka, and S. Aramaki (2001), Differentiation processes of Deccan Trap basalts: Contribution from geochemistry and experimental petrology, *J. Petrol.*, 42(12), 2175–2195, doi:10.1093/petrology/42.12.2175.
- Sastri, V., B. Venkatachala, and V. Narayanan (1981), The evolution of the east coast of India, *Palaeogeogr. Palaeoclimatol. Palaeoecol.*, 36(1–2), 23–54, doi:10.1016/0031-0182(81)90047-X.
- Sayles, F. L., E. T. Manheim, and L. S. Waterman (1973), Interstitial water studies on small core samples, Leg 15, in *Initial Rep. Deep Sea Drill. Proj.*, vol. 20, edited by B. C. Heezen and I. D. MacGregor, pp. 783–804, U.S. Gov. Print. Off., Washington, D. C., doi:10.2973/dsdp.proc.9.117.1972.
- Schenau, S., H. Passier, G. Reichart, and G. De Lange (2002), Sedimentary pyrite formation in the Arabian Sea, *Mar. Geol.*, 185(3–4), 393–402, doi:10.1016/S0025-3227(02)00183-4.
- Schmidt, M., C. Hensen, T. Morz, C. Muller, I. Grevemeyer, K. Wallmann, S. Mau, and N. Kaul (2005), Methane hydrate accumulation in “Mound 11” mud volcano, Costa Rica forearc, *Mar. Geol.*, 216(1–2), 83–100, doi:10.1016/j.margeo.2005.01.001.
- Shen, Y., and R. Buick (2004), The antiquity of microbial sulfate reduction, *Earth Sci. Rev.*, 64(3–4), 243–272, doi:10.1016/S0012-8252(03)00054-0.
- Sheth, H. C., J. J. Mahoney, and D. Chandrasekharam (2004), Geochemical stratigraphy of Deccan flood basalts of the Bijasan Ghat section, Satpura Range, India, *J. Asian Earth Sci.*, 23(1), 127–139, doi:10.1016/S1367-9120(03)00116-0.
- Sim, M. S., T. Bosak, and S. Ono (2011), Large sulfur isotope fractionation does not require disproportionation, *Science*, 333, 74–77, doi:10.1126/science.1205103.
- Skyring, G. (1987), Sulfate reduction in coastal ecosystems, *Geomicrobiol. J.*, 5(3), 295–374, doi:10.1080/01490458709385974.
- Solomon, E. A., A. J. Spivack, M. Kastner, M. Torres, D. Borole, G. Robertson, and H. C. Das (2008), Hydrogeochemical and structural controls on heterogeneous gas hydrate distribution in the K-G basin offshore, India, paper presented at the 6th International Conference on Gas Hydrates (ICGH 2008), Vancouver, British Columbia, Canada.
- Solomon, E. A., A. J. Spivack, M. Kastner, M. E. Torres, and G. Robertson, (2014), Gas hydrate distribution and carbon sequestration through coupled microbial methanogenesis and silicate weathering in the Krishna-Godavari basin, offshore India, *Mar. Petrol. Geol.*, 58, 233–253, doi:10.1016/j.marpetgeo.2014.08.020.
- Strauss, H. (1997), The isotopic composition of sedimentary sulfur through time, *Palaeogeogr. Palaeoclimatol. Palaeoecol.*, 132, 97–118, doi:10.1016/S0031-0182(97)00067-9.
- Strauss, H., et al. (2012), Sulphur diagenesis in the sediments of the Kiel Bight, SW Baltic Sea, as reflected by multiple sulfur isotopes, *Isotopes Environ. Health Stud.*, 48, 166–179, doi:10.1080/10256016.2012.648930.
- Treude, T., J. Niggemann, J. Kallmeyer, P. Wintersteller, C. J. Schubert, A. Boetius, and B. B. Jørgensen (2005), Anaerobic oxidation of methane and sulfate reduction along the Chilean continental margin, *Geochim. Cosmochim. Acta*, 69(11), 2767–2779, doi:10.1016/j.gca.2005.01.002.
- Treude, T., S. Krause, J. Schweers, A. W. Dale, R. Coffin, and L. J. Hamdan (2014), Sulfate reduction and methane oxidation activity below the sulfate-methane transition zone in Alaskan-Beaufort continental margin sediments: Implications for deep sulfur cycling, *Geochim. Cosmochim. Acta*, 144, 217–237, doi:10.1016/j.gca.2014.08.018.
- Ussler, W., III, and C. K. Paull (2008), Rates of anaerobic oxidation of methane and authigenic carbonate mineralization in methane-rich deep-sea sediments inferred from models and geochemical profiles, *Earth Planet. Sci. Lett.*, 266(3–4), 271–287, doi:10.1016/j.epsl.2007.10.056.
- Wang, J., Q. Chen, Q. Wei, X. Wang, Q. Li, and Y. Gao (2008), Autogenous pyrites and their stable sulfur isotopes in sediments from IODP 311 on Cascadia margin, Northeastern Pacific, paper presented at the International Conference on Gas Hydrates, Vancouver, B. C., Canada.
- Wehrmann, L. M., S. P. Templer, B. Brunner, S. M. Bernasconi, L. Maignien, and T. G. Ferkel (2011), The imprint of methane seepage on the geochemical record and early diagenetic processes in cold-water coral mounds on Pen Duick Escarpment, Gulf of Cadiz, *Mar. Geol.*, 282(1–2), 118–137, doi:10.1016/j.margeo.2010.08.005.
- Werne, J., T. Lyons, D. Hollander, M. Formolo, and J. Sinninghe Damsté (2003), Reduced sulfur in euxinic sediments of the Cariaco Basin: Sulfur isotope constraints on organic sulfur formation, *Chem. Geol.*, 195(1–4), 159–179, doi:10.1016/S0009-2541(02)00393-5.
- Westrich, J., and R. Berner (1988), The effect of temperature on rates of sulfate reduction in marine sediments, *Geomicrobiol. J.*, 6(2), 99–117, doi:10.1080/01490458809377828.
- Whiticar, M. J. (1999), Carbon and hydrogen isotope systematics of bacterial formation and oxidation of methane, *Chem. Geol.*, 161(1–3), 291–314, doi:10.1016/S0009-2541(99)00092-3.
- Wilkin, R., and H. Barnes (1997), Formation processes of frambooidal pyrite, *Geochim. Cosmochim. Acta*, 61(2), 323–339, doi:10.1016/S0016-7037(96)00320-1.
- Wortmann, U., S. Bernasconi, and M. Böttcher (2001), Hypersulfidic deep biosphere indicates extreme sulfur isotope fractionation during single-step microbial sulfate reduction, *Geology*, 29(7), 647–650, doi:10.1130/0091-7613(2001)029.
- Yoshinaga, M. Y., T. Holler, T. Goldhammer, G. Wegener, J. W. Pohlman, B. Brunner, M. M. Marcel, M. M. Kuypers, K.-W. Hinrichs, and M. Elvert (2014), Carbon isotope equilibration during sulphate-limited anaerobic oxidation of methane, *Nat. Geosci.*, 7, 190–194, doi:10.1038/ngeo2069.
- Zabel, M., and H. D. Schulz (2001), Importance of submarine landslides for non-steady state conditions in pore water system-lower Zaire (Congo) deep-sea fan, *Mar. Geol.*, 176, 87–99, doi:10.1016/S0025-3227(01)00164-5.
- Zopfi, J., T. Ferkel, and H. Fossing (2004), Distribution and fate of sulfur intermediates—Sulfite, tetrathionate, thiosulfate, and elemental sulfur—in marine sediments, *GSA Spec. Pap.*, 379, 97–116.